Available online at www.sciencedirect.com

ScienceDirect

Geochimica et Cosmochimica Acta 149 (2015) 131–151

Geochimica et Cosmochimica Acta

www.elsevier.com/locate/gca

The magnesium isotope ($\delta^{26}Mg$) signature of dolomites

A. Geske [a], R.H. Goldstein [b], V. Mavromatis [c], D.K. Richter [a], D. Buhl [a], T. Kluge [d], C.M. John [d], A. Immenhauser [a,*]

[a] Ruhr-University Bochum, Institute for Geology, Mineralogy and Geophysics, Universitätsstraße 150, D-44801 Bochum, Germany
[b] University of Kansas, Department of Geology, 1475 Jayhawk Blvd., Lawrence, KS 66045, USA
[c] Institute of Applied Geosciences, Graz University of Technology, 8010 Graz, Austria
[d] Imperial College London, Department of Earth Science and Engineering, Prince Consort Road, SW7 2BP London, United Kingdom

Received 1 August 2014; accepted in revised form 1 November 2014; available online 13 November 2014

Abstract

Dolomite precipitation models and kinetics are debated and complicated due to the complex and temporally fluctuating fluid chemistry and different diagenetic environments. Using well-established isotope systems ($\delta^{18}O$, $\delta^{13}C$, $^{87}Sr/^{86}Sr$), fluid inclusions and elemental data, as well as a detailed sedimentological and petrographic data set, we established the precipitation environment and subsequent diagenetic pathways of a series of Proterozoic to Pleistocene syn-depositional marine evaporative (sabkha) dolomites, syn-depositional non-marine evaporative (lacustrine and palustrine) dolomites, altered marine ("mixing zone") dolomites and late diagenetic hydrothermal dolomites. These data form the prerequisite for a systematic investigation of dolomite magnesium isotope ratios ($\delta^{26}Mg_{dol}$). Dolomite $\delta^{26}Mg$ ratios documented here range, from $-2.49‰$ to $-0.45‰$ ($\delta^{26}Mg_{mean} = -1.75 \pm 1.08‰$, $n = 42$). The isotopically most depleted end member is represented by earliest diagenetic marine evaporative sabkha dolomites ($-2.11 \pm 0.54‰$ 2σ, $n = 14$). In comparing ancient compositions to modern ones, some of the variation is probably due to alteration. Altered marine ($-1.41 \pm 0.64‰$ 2σ, $n = 4$), and earliest diagenetic lacustrine and palustrine dolomites ($-1.25 \pm 0.86‰$ 2σ, $n = 14$) are less negative than sabkha dolomites but not distinct in composition. Various hydrothermal dolomites are characterized by a comparatively wide range of $\delta^{26}Mg$ ratios, with values of $-1.44 \pm 1.33‰$ (2σ, $n = 10$). By using fluid inclusion data and clumped isotope thermometry (Δ_{47}) to represent temperature of precipitation for hydrothermal dolomites, there is no correlation between fluid temperature (~100 to 180 °C) and dolomite Mg isotope signature ($R^2 = 0.14$); nor is there a correlation between $\delta^{26}Mg_{dol}$ and $\delta^{18}O_{dol}$. Magnesium-isotope values of different dolomite types are affected by a complex array of different Mg sources and sinks, dissolution/precipitation and non-equilibrium fractionation processes and overprinted during diagenetic resetting. Further progress on the use of $\delta^{26}Mg_{dol}$ as a proxy will require new theoretical and experimental data for $\Delta^{26}Mg_{fluid\text{-}dol}$ that includes dehydration effects of the free Mg aquo ion versus fluid temperature. In ancient diagenetic systems, complex variables must be considered. These include fluid chemistry and physical properties, Mg sources and sinks, temporal changes during precipitation and post-precipitation processes including open and closed system geochemical exchange with ambient fluids. All of these factors complicate the application of $\delta^{26}Mg_{dol}$ as proxy for their depositional or diagenetic environments. Nevertheless, the data shown here also indicate that $\delta^{26}Mg_{dol}$ can in principle be interpreted within a detailed framework of understanding.

* Corresponding author. Tel.: +49 (0)234 3228250.
E-mail address: adrian.immenhauser@rub.de (A. Immenhauser).

http://dx.doi.org/10.1016/j.gca.2014.11.003
0016-7037/

1. INTRODUCTION

Dolomite is a major carbonate mineral throughout Earth history, but one that remains debated in terms of its precipitation and alteration kinetics to the present day. Moreover, dolostones have great economic significance as reservoir rock facies worldwide (Warren, 2000). Dolomite formation models relate to specific precipitation and diagenetic environments and include complex and variable fluid chemistries. Conventionally, dolomite formation and alteration environments are explored via the study of more traditional stable and radiometric isotope systems, elemental abundances and ratios as well as petrographic and geothermometric approaches (Last, 1990; Vasconcelos et al., 1995; Budd, 1997; Warren, 2000; Machel and Lonnee, 2002; Machel, 2004; Bontognali et al., 2010; Zhang et al., 2012). Magnesium in turn is a major element in dolomite and thus, the study of dolomite magnesium isotope ratios ($\delta^{26}Mg_{dol}$) is a potentially promising research field, but one that is insufficiently explored. Here we suggest that dolomite Mg isotope ratios must be added to the list of proxies when dealing with recent and fossil dolomites. The objective is to develop the framework by which carbonate geologists and geochemists will be able to understand and interpret $\delta^{26}Mg$ in dolomites and perhaps marine carbonates more widely. This is important because dolomite forms an essential Mg sink and is a main control on $\delta^{26}Mg_{seawater}$. Moreover, Mg is an element that is critically involved in the carbon cycle in general (see discussion in Tipper et al., 2006a,b,c and Pogge von Strandmann et al., 2014). This work is motivated by the increasing number of studies dealing with the $\delta^{26}Mg$ signature of marine and terrestrial carbonate dissolution and precipitation environments (De Villiers et al., 2005; Buhl et al., 2007; Hippler et al., 2009; Kisakurek et al., 2009; Higgins and Schrag, 2010, 2012; Immenhauser et al., 2010; Pokrovsky et al., 2011; Wombacher et al., 2011; Riechelmann et al., 2012a, 2012b; Shirokova et al., 2013; Mavromatis et al., 2013, 2014; Wang et al., 2013; Beinlich et al., 2014). Conversely, recent studies on sedimentary rocks, biominerals as well as igneous and metamorphic rocks or precipitation experiments document a wide range of $\delta^{26}Mg$ corresponding to different mineralogies, crystal structures, kinetics and precipitation environments (Galy et al., 2002; Young and Galy, 2004; De Villiers et al., 2005; Tipper et al., 2006a,b,c, 2012; Buhl et al., 2007; Bolou-Bi et al., 2007, 2009; Pogge von Strandmann et al., 2008a,2008b, 2014; Huang et al., 2009, 2012; Chakrabarti and Jacobsen, 2010; Jacobson et al., 2010; Liu et al., 2010; Teng et al., 2010; Wimpenny et al., 2011, 2014a,b; Yoshimura et al., 2011, and others).

Nevertheless, compared to other carbonate minerals, the $\delta^{26}Mg$ composition of the wide range of dolomite types is still underexplored and published data of well constrained $\delta^{26}Mg_{dol}$ ratios are scattered in the literature (Galy et al., 2002; Higgins and Schrag, 2010; Pokrovsky et al., 2011; Geske et al., 2012; references in Li et al., 2012b; Azmy et al., 2013; Lavoie et al., 2014; Mavromatis et al., 2014). This is in part related to the difficulties to experimentally precipitate dolomite under ambient conditions (Vasconcelos et al., 1995; Zhang et al., 2012; Roberts et al., 2013), and in part to the inaccessibility of many natural dolomite-precipitating environments. Consequently, it is not surprising that studies dealing with for example burial dolomitization fluid parameters and factors controlling $\Delta^{26}Mg_{fluid\text{-}solid}$ in basinal and hydrothermal precipitation and subsequent diagenetic alteration environments are scarce (Geske et al., 2012; Azmy et al., 2013). Similarly, the potential of earliest diagenetic marine evaporitic dolomites (Geske et al., 2012) or Precambrian cap dolomites (Pokrovsky et al., 2011; Kasemann et al., 2014) as archives of past seawater $\delta^{26}Mg$ signatures and, more generally, the global magnesium cycle (Tipper et al., 2006b,c) requires further exploration.

The aim of this study is to (i) systematically investigate and document $\delta^{26}Mg_{dol}$ of various early and late diagenetic dolomite types from numerous settings and time intervals worldwide and to (ii) place these findings in a mechanistic context of syn- and post-precipitation physico-chemical parameters affecting $\Delta^{26}Mg_{fluid\text{-}dol}$ in near-surface and burial dolomite-precipitating environments. Magnesium isotope data shown here are compared to complementary sedimentological, petrographical, geochemical, mineralogical and crystallographical data and discussed in the context of their respective environments of dolomite precipitation. The overarching goal is to test the hypothesis that $\delta^{26}Mg_{dol}$ can significantly contribute to our understanding of dolomitization and dolomite-precipitation environments.

2. STUDY SITES, MATERIALS AND DOLOMITE ORIGIN

Geochemically well-characterized dolomites were obtained from field sites in Germany, Greece, Austria, Italy, Belgium, Algeria, Angola, the Bahamas, Canada, the UAE and the USA. Refer to Fig. 1a, b and Appendix A1 for detailed information (Appendix A). Dolomite types, their formation ages, sampling locations, depositional- and diagenetic environments and petrography, are placed in context with $\delta^{26}Mg$ values and constrained by strontium ($^{87}Sr/^{86}Sr$) carbon ($\delta^{13}C$) and oxygen ($\delta^{18}O$) isotope ratios, fluid inclusion data, clumped isotope thermometry, cathodoluminescence analyses and major/trace element concentrations. This is important as many of the previous studies lack this systematic background data rendering the interpretation of the resulting data difficult.

This study uses well-described examples of (i) marine evaporitic (sabkha), (ii) lacustrine/palustrine, (iii) altered marine (formerly "mixing zone") and (iv) hydrothermal (burial, basinal) dolomites from the Proterozoic and the Phanerozoic. Dolomite types refer to different settings for precipitation including: lacustrine (saline lake), palustrine (swamp), inland playa (coast), sabkha (coast), altered marine (coast) and hydrothermal (Fig. 2). We apply the definitions of Briere (2000) for playa and sabkha settings. Many of the dolomites analyzed were previously studied using multiple techniques, and corresponding references are listed in the digital Appendix A1.

Currently applied dolomitization models include syn-sedimentary microbially mediated precipitation (mainly

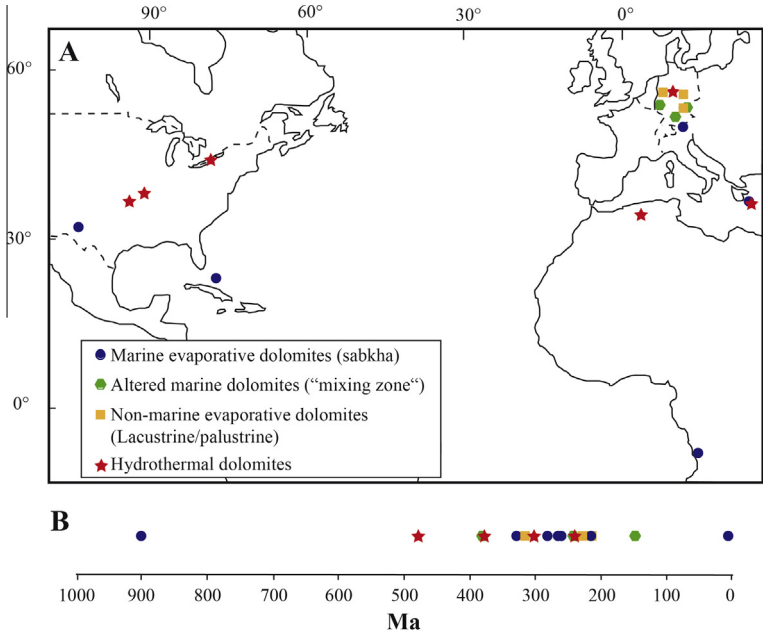

Fig. 1. (A) Map indicating dolomite sampling sites in Germany, Greece, Austria, Italy, Belgium, Algeria, Angola, Bahamas, Canada and the USA. Note color key to different dolomite types. (B) Time scale [Ma] indicates age of host rock whilst dolomitization might range from penecontemporaneous to significantly younger than the age of the host rock.

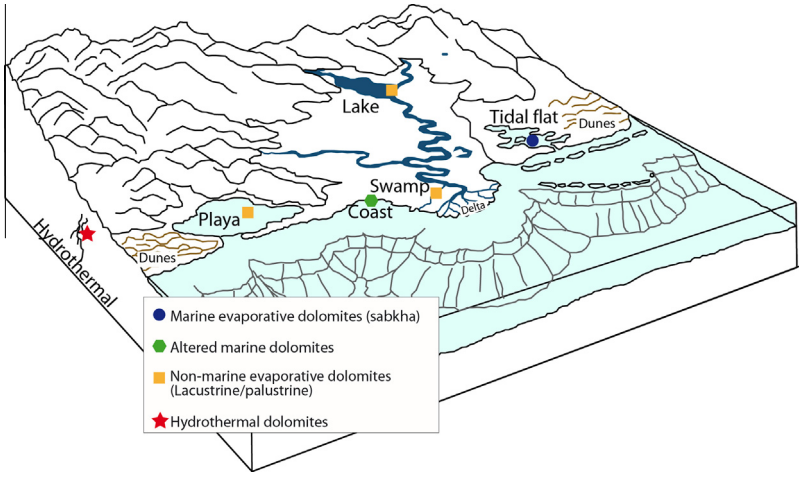

Fig. 2. Conceptual depositional/diagenetic environments of dolomites studied including sabkha dolomites (blue dots), altered marine dolomites (green hexagons), lacustrine (coorong) and palustrine dolomites (yellow squares) and hydrothermal dolomites (red stars) (redrawn after Jones and Xiao, 2005). Dunes reflect arid climate conditions, whereas river beds symbolize humid climate. (For interpretation of the references to color in this figure legend, the reader is referred to the web version of this article.)

marine and lacustrine evaporative; e.g., Van Lith et al., 2003b), marine abiogenic dolomitization (e.g., Humphrey and Quinn, 1989), shallow/deep low-temperature reflux (e.g., Jones and Xiao, 2005), deep burial thermo-chemical sulfate reduction (Machel, 1987) and hydrothermal (burial) dolomite (e.g., Davies and Smith, 2006). Three of the four dolomite models discussed here are widely accepted and include (i) marine evaporative dolomite in marine evaporative (sabkha) settings; (ii) non-marine evaporative dolomite in lacustrine/palustrine settings (fluvial, lacustrine) and (iii) hydrothermal dolomite (formation brines). For discussions of these models refer to Tucker and Wright (1990), Last (1990, 2012), Budd (1997), Mazzullo (2000), Warren (2000), Machel (2004) or Richter et al. (2014). In coastal settings, including marine evaporative and marine alteration settings, the main magnesium source for dolomite formation is modified seawater (diluted or hypersaline). Additional magnesium sources include evaporites,

Mg-bearing silicates and the (carbonate) host rock itself (Bolou-Bi et al., 2009; Huang et al., 2013). In coastal settings (swamp, playa) dolomitization takes place in (ephemeral) lakes under the influence of continental alkaline groundwater (Morrow, 1982). In burial settings, hydrothermal fluids, potentially ascending via diverse lithologies including crystalline basement, mafic and ultramafic volcanics and (carbonate) host rock, reflect the major source of magnesium for dolomite precipitation. This is of importance, as in burial dolomite environments, rock–water interaction is highly significant and must not be compared with the fluid-dominated marine environment.

In contrast, the "mixing-zone dolomitization model" is controversial (Machel, 2004; Li et al., 2013) and there is no simple explanation. The precipitation of what is here labeled "altered marine dolomites", took place in shallow-water carbonate platform margin environments near the sediment surface and subsequently progressed into the underlying sediments (sample Prüstr.4: Richter, 1974; sample Moggast1: Meyer and Schmidt-Kaler, 1990). Subsequently, dolomitized units were overprinted by low temperature non-marine fluids. In the context of this study, this model refers to reefal dolomites from the Swabian Alb (Koch and Schorr, 1986), the Francian Alb (Richter et al., 2003b), the Eifel area (Richter, 1974) in Germany and to Triassic Contrin Formation dolomites in the south Tyrolean Dolomites in Italy (Bosellini, 1998).

3. METHODS

Dolomitization fluid chemistry and precipitation/diagenetic environments were assessed by analyzing oxygen ($\delta^{18}O$), carbon ($\delta^{13}C$) and strontium ($^{87}Sr/^{86}Sr$) isotope ratios and as well as major and trace element (Ca, Mg, Fe, Mn, Sr) abundances. Mineralogical analyses were performed using standard petrographic (polarizing microscope, cathodoluminescence) and X-ray diffraction techniques. Fluid inclusion data are from Hiemstra and Goldstein (2004, 2014). Clumped isotope analyses were performed on six hydrothermal dolomite samples to determine their temperature of precipitation.

3.1. Sampling strategy

Dolomite powder, approximately 30 mg, was extracted from 38 specimens (including 42 samples) each with a hand brace (Dremel). Because of the large sample size requirements, most of the dolomite samples had to consist of more than one dolomite phase. Under cathodoluminescence, up to ten phases/zones of mainly late diagenetic hydrothermal dolomites form complex aggregates and growth zones whilst early diagenetic phases are petrographically often more uniform or mottled. The limitation of such bulk sampling, including several dolomite phases, must be emphasized as likely resulting in physical mixtures of dolomites from different diagenetic settings. The implication of this is that it might be difficult to relate a specific bulk magnesium isotope signature to a specific, volumetrically insignificant dolomite phase in a given sample. The pragmatic approach applied here is that powder samples were taken from areas where the targeted dolomite type formed >80% of bulk carbonate as evident from detailed thin section analysis. Samples containing calcite were treated with 1 M acetic acid or 0.27 M Di-Na-EDTA to remove the calcite phase.

3.2. Crystallographic and microscopic analysis of dolomites

In order to constrain the dolomite stoichiometry and degree of order (R), all samples were analyzed with a Phillips ẊPert MPD Theta–Theta X-ray Diffractometer using Cu Kα radiation at 45 kV and 40 mA. The scanning range was 20° to 40° (2θ) with a step of 0.025° (2θ) and an acquisition time of 11 s per step. A graphite secondary monochromator was used to minimize the background noise. The $CaCO_3$ content in mol-% was calculated using the equation of (Lumsden, 1979); the degree of order (R) of each dolomite was calculated with the equation of Füchtbauer and Goldschmidt (1965), Füchtbauer and Richter (1988) and Hardy and Tucker (1988).

Cathodoluminescence analysis (CL) was performed to characterize the different dolomite generations found within thin sections. A total of twenty-eight thin sections sputtered with gold were examined under transmitted light and cathodoluminescence microscopy using a hot stage HC1-LM facility (Neuser et al., 1996). The instrument is linked to a Kappa DX 30C video camera system for recording digital images and with an EG&G triple grating spectrograph connected to a liquid-N_2 cooled CCD-detector. Operating conditions were about 5 and 10 μA/mm^2 and 14 kV with a beam current of 0.1–0.2 mA. Integration times for luminescence-spectra were commonly between 10 and 60 s. For more details refer to Richter et al. (2003a).

3.3. Geochemical analysis of dolomites

3.3.1. Magnesium isotope ($\delta^{26}Mg$) analysis

For $\delta^{26}Mg$ analysis, ~0.5 mg of powder was weighed. The extraction and purification process involves several steps. First, the samples were dissolved in 1 ml 6 M HCl (supra pure) and dried on a hot plate at >100 °C. The samples were treated with 1 ml H_2O_2–HNO_3 1:1 mixture to destroy organic compounds and minimize potential interferences related to complexation of cations. The samples were subsequently dried on a hot plate (60 °C) and then re-dissolved in 1 ml 1.25 N HCl. The Mg fraction, typically 50 μg, was recovered using BioRad ion exchange resin AG50W-X12 (200–400 mesh) and quartz glass columns. The column elution pattern was determined for each column using an IAPSO seawater test solution (diluted 1:1). The Mg yield exceeds 95%.

The analytical method is described in detail by Immenhauser et al. (2010). A 500 ppb Mg solution in 3.5% HNO_3 was measured on a Thermo Fisher Scientific Neptune MC-ICP-MS. The sample Mg concentration was kept within ±15% of the standard, which proved to minimize potential isobaric interferences from matrices (Galy et al., 2001). A positive effect on signal stability and reduction of matrix interferences was achieved by combining two desolvating systems (ApexIR (ESI), Aridus (Cetac)) and the

low-resolution slit of the Thermo Fisher Scientific Neptune. The standard sample bracketing technique was applied to calculate the $\delta^{25}Mg$ and $\delta^{26}Mg$ values (‰). Each measurement value comprises a sequence of 5 repetitions of sample measurements representing 250 ratios (each ratio consists of 4.194 s integration time and 3.0 s idle time). The beam intensity for mass 24 is typically 10 V per 100 ppb Mg. The average signal stability is 0.01–0.005 V.

The reproducibility of Mg isotope measurements was assessed using samples of (i) the internal carbonate standard RUB (Solnhofen Plattenkalk), (ii) the mono elemental solution Cambridge1, (iii) IAPSO seawater and (iv) a dolomite sample (HDK7). Each standard sample was processed identically, except different ion exchange columns were used. The RUB standard samples resulted in a $\delta^{26}Mg$ value of $-3.66‰ \pm 0.06$ (2σ). For the time interval 2005–2012, the $\delta^{26}Mg_{Cambridge1}$ value is $-2.57‰ \pm 0.06$ 2σ ($n = 431$). Between 2011 and 2012 $\delta^{26}Mg_{Cambridge1}$ resulted in $-2.58‰ \pm 0.06$ 2σ ($n = 92$). These results are indistinguishable from published values ($\delta^{25}Mg_{Cambridge1} = -2.58 \pm 0.14‰$ 2σ, $n = 35$; Galy et al., 2003; Young and Galy, 2004). The magnesium isotope composition of IAPSO seawater and dolomite HDK7 resulted in $\delta^{26}Mg$ values of $-0.81 \pm 0.06‰$ 2σ ($n = 130$) and $-2.02 \pm 0.02‰$ 2σ ($n = 5$), respectively; see also Foster et al., 2010). The total blank for the complete analysis was 10 ng Mg, which represents an average blank-to-sample ratio of $2 * 10^{-4}$.

3.3.2. Strontium ($^{87}Sr/^{86}Sr$) isotope analysis

Dolomite $^{87}Sr/^{86}Sr$ ratios indicate the strontium source of burial fluids and alteration effects (Faure and Powell, 1972). The Sr fraction (500 ng per analysis) was separated twice using quartz glass columns, filled with BioRad ion exchange resin AG50W-X8. The $^{87}Sr/^{86}Sr$ ratio was determined with a 7 collector Thermal Ionisation Mass spectrometer (TIMS) MAT 262 in 3 collector dynamic mode. As standard reference materials NIST NBS 987 and USGS EN-1 were used. The total blank for Sr isotope analysis, including chemical separation and loading blank, is 1.5 ng. The reproducibility of carbonate extraction and measurement was tested with the USGS modern bivalve carbonate EN-1. Resulting in an average $^{87}Sr/^{86}Sr$ value of 0.709160 ± 0.000027 2σ ($n = 209$). The mass spectrometric reproducibility of Sr measurements was assessed with NBS987, which was directly loaded onto a Re filament resulting in an average value of 0.710240 ± 0.000034 2σ ($n = 233$), which agree with mean values of NBS987 of McArthur et al. (2001; NBS987 = 0.710247). Details of the analytical technique are described by e.g., Faure and Powell (1972).

3.3.3. Carbon ($\delta^{13}C$) and oxygen ($\delta^{18}O$) isotope analysis

Carbon and oxygen isotope signatures were analyzed on sample aliquots (0.4 ± 0.03 mg) to define the dolomitizing fluid on a ThermoFinnigan MAT 253 coupled to a Gasbench II and a PAL auto sampler (GasIRMS). All isotope ratios are reported as per mil (‰) deviation from the Vienna-Pee Dee Formation belemnite (V-PDB) standard. The carbonate standards NBS 19, IAEA CO-1 and CO-8 and an internal standard (RUB standard) were used as a reference. The standard deviations (2σ) of 8 RUB standards measured within these sample sequences are 0.06‰ and 0.08‰ for C- and O isotopic measurements, respectively. The measured $\delta^{13}C$ values for standards CO-1, CO-8 and NBS19 are $2.48 \pm 0.04‰$, $-5.75 \pm 0.02‰$ and $1.94 \pm 0.03‰$ in comparison to the certificated values of 2.48‰, −5.75‰ and 1.95‰, respectively. The measured $\delta^{18}O$ values for standards CO-1, CO-8 and NBS19 are -2.44 ± 0.07, -22.67 ± 0.04 and -2.13 ± 0.04 in comparison to the certificated values of −2.44‰, −22.67‰ and −2.20‰ respectively. The mean value of the measured samples and the certificated values of CO-1 and CO-8 are equal, as all samples and standards are normalized to CO-1 and CO-8.

3.3.4. Clumped isotope (Δ_{47}) analysis

Six samples of pure dolomite aliquots from the hydrothermal dolomites were selected for clumped isotope analysis (T). Five to six mg of powdered dolomite was reacted for 40 min in phosphoric acid held at 90 °C. The liberated CO_2 gas was purified by passage through a conventional vacuum line with multiple cryogenic traps and a Porapak-Q trap held at −35 °C (Dennis and Schrag, 2010). CO_2 gas was analyzed using two Thermo Finnigan MAT-253 gas source isotope ratio mass spectrometers configured to measure masses 44 through 49 at the Qatar Stable Isotopes Laboratory at Imperial College, London, UK. Analytical protocols and corrections for non-linearity follow Huntington et al. (2009) and the data are reported in the "carbon dioxide equilibrated scale" (CDES) of Dennis et al. (2011). An acid correction factor of +0.081‰ was added to all measurements of $\Delta_{47\ CDES}$ following Ferry et al. (2011). Masses 48 and 49 were monitored to check for possible sample contamination following (Affek and Eiler, 2006) and Huntington et al. (2009, 2011). Each sample was measured at least three times to improve counting statistics. The $\Delta_{47\ CDES}$ reproducibility is ±0.03‰ based on regular analysis of Carrara marble and an internal gas standard (BOC, CO_2 research grade 100.000%). The Carrara marble $\Delta_{47\ CDES}$ value is $0.390 \pm 0.006‰$ (S.E., $n = 26$) and $0.386 \pm 0.003‰$ (S.E., $n = 49$) for both mass spectrometers used. The $\Delta_{47\ CDES}$ values were converted to temperature solving numerically for the calibration of Passey and Henkes (2012):

$$\Delta_{47}^{eq} = \frac{-3.407 \times 10^9}{T^4} + \frac{2.365 \times 10^7}{T^3} + \frac{2.607 \times 10^3}{T^2} + \frac{5.880}{T} + 0.268 \quad (1)$$

3.3.5. Elemental (Ca, Mg, Fe, Mn, Sr and Ba) analyses

In order to complement isotope data, major and trace elemental analysis was performed from aliquots of all samples. 1.50 ± 0.15 mg dolomite was dissolved in 3 M HNO_3 and subsequently diluted with 2 ml deionized H_2O (>18.2 MΩ cm^{-1}). The concentrations of Ca, Mg, Fe, Mn, Sr and Ba were measured with an inductively coupled plasma optical emission spectrometer (ICP-OES, Thermo Fisher Scientific iCAP 6500 DUO). BSC-CRM-512 and

BSC-CRM-513 were used as reference materials. All major and trace elemental results are reported in ppm (parts per million). The 1σ-reproducibility on 111 standard samples for Mg is 0.18% and 0.36%, for Ca is 0.081% and 0.002%, for Sr is 22 ppm and 1 ppm, for Fe is 17 ppm and 12 ppm, for Mn is 1 ppm and 1 ppm for BSC-CRM-512 and for BCS-CRM-513, respectively.

4. RESULTS

4.1. Petrographic and crystallographic characterization of dolomites

All dolomites studied (Table 1) here yield between 48 and 56 mol percent $CaCO_3$ (Table 2). We follow the terminology proposed by Gregg and Sibley (1984) and Sibley and Gregg (1987) to describe dolomite textures of samples analyzed here.

The earliest diagenetic dolostones (marine evaporative sabkha dolomites and lacustrine as well as palustrine dolomites) have very small to crypto-crystalline grain size (<20 μm), unimodal nonplanar (anhedral to subhedral) crystals, well preserved relict sediment textures/structures and fossils and the lack of appreciable porosity. The sabkha dolomicrites show homogeneous compositional and textural character alternating with typical "birdseyes", i.e., spar-filled primary pore-space (Murray, 1960; Drummond, 1964) and mud cracks. Silicified sulfate nodules, equivalents of "chicken wire" structure (Purser and Sibold, 1973; McKenzie, 1981), within micritic dolomite layers and anhydrite/gypsum was found in many thin sections. Oncoids and stromatoids are common in the sabkha dolomicrites and are evidence for cyanobacterial biofilms typifying peritidal environments. Cathodoluminescence analysis revealed beige, light orange and bright red luminescence colors (Fig. 3B). The earliest diagenetic sabkha dolomites show a crystallographic ordering of Ca and Mg expressed by a low crystallographic degree of order (R = I (015/110) of about 0.57. Playa dolomites contain anhydrite and shrinkage cracks indicative of a saline/arid environment. Lake dolomicrites display depositional relict laminae (Fig. 3E). These dolomites show yellow to beige

Table 1
Dolomite geochemistry, including magnesium isotope data, clumped isotope data and circumstantial geochemical data.

Nr.	Sample	$\delta^{26}Mg_{DSM3}$ [‰]	±2σ	$\delta^{25}Mg_{DSM3}$ [‰]	±2σ	$^{87}Sr/^{86}Sr$	±2σ	$\delta^{13}C_{V\text{-}PDB}$ [‰]	±σ	$\delta^{18}O_{V\text{-}PDB}$ [‰]	±σ	Δ_{47}	±1S.E.	$T_{dolomitization\ fluid}$ [°C]*
														Based on Δ_{47} (Passey and Henkes, 2012) Eq. (1)
Marine evaporative dolomite (sabkha)														
1	2a10	−2.49	0.08	−1.29	0.04			3.8	0.03	−2.2	0.03			
2	2a12	−2.44	0.06	−1.27	0.04	0.707715	0.000006	3.9	0.03	−1.7	0.04			
3	HDK51	−1.99	0.07	−1.03	0.03	0.708002	0.000006	2.6	0.03	−1.4	0.05			
4	1b23	−2.24	0.10	−1.16	0.05	0.707178	0.000006	4.8	0.03	−1.1	0.05			
5	Bel1a	−2.20	0.06	−1.14	0.03	0.707782	0.000007	0.6	0.02	−3.4	0.02			
6	Bel1b	−2.20	0.06	−1.14	0.03			0.6	0.05	−2.8	0.03			
7	Oo	−1.70	0.03	−0.90	0.01	0.707485	0.000006	7.2	0.04	1.5	0.03			
8	Oom	−1.71	0.02	−0.89	0.02			7.1	0.02	1.8	0.01			
9	Kri	−2.03	0.06	−1.08	0.02	0.708277	0.000007	4.4	0.02	−0.8	0.02			
10	Angola1	−1.67	0.05	−0.87	0.03			1.3	0.02	−12.4	0.02			
11	B30	−2.05	0.02	−1.07	0.01			0.7	0.05	0.3	0.05			
12–14	B31a–c ($n = 3$)	−2.28	0.23	−1.12	0.12	0.708695	0.000118	2.0	0.08	1.1	0.80			
Mean	(±2σ)	−2.11	0.54	−1.10	0.27	0.708030	0.001084	3.1	4.40	−1.4	7.20			n.d.
Mixing zone dolomite														
15	Moggast1	−1.86	0.04	−0.96	0.01	0.707185	0.000007	3.0	0.02	−3.5	0.05			
16	Hund1	−1.30	0.05	−0.68	0.03	0.707212	0.000007	2.8	0.03	−4.6	0.03			
17	Contrin2	−1.38	0.07	−0.73	0.03	0.707931	0.000007	3.1	0.03	−4.2	0.04			
18	Prüstr. 4	−1.10	0.05	−0.57	0.03			−0.6	0.05	−4.4	0.03			
Mean	(±2σ)	−1.41	0.64	−0.74	0.33	0.707443	0.000846	2.1	3.60	−4.2	1.00			n.d.
Non-marine evaporative dolomite (Lacustrine/palustrine)														
19	Ofeu3	−2.08	0.09	−1.08	0.04	0.709281	0.000007	−7.6	0.03	−8.8	0.04			
20–21	Blei 2a. 2b ($n = 2$)	−1.89	0.12	−0.99	0.02			−2.7	0.02	−3.1	0.03			
22	StBe20	−1.51	0.04	−0.81	0.02	0.707429	0.000007	−1.4	0.03	3.7	0.04			
23–32	Swamp dol ($n = 10$)	−1.06	0.61	−0.55	0.32	0.708880	0.000151	−13.5		−7.3				
Mean	(±2σ)	−1.25	0.86	−0.66	0.45	0.708617	0.001631	−11.0	12.90	−5.3	7.30			n.d.
Hydrothermal dolomite														
33	RSD-Dol	−1.67	0.05	−0.87	0.03	0.707749	0.000007	3.2	0.03	−9.5	0.03			
34	5a1	−2.22	0.05	−1.15	0.04	0.707885	0.000007	3.6	0.03	−4.5	0.05	0.451	0.008	157 ± 8
35	5e3	−2.18	0.05	−1.13	0.01			3.4	0.04	−3.3	0.03			
36	Letmathe1	−0.45	0.04	−0.23	0.02	0.708550	0.000007	2.7	0.03	−11.1	0.03	0.480	0.012	132 ± 9
37	PH37	−0.61	0.03	−0.31	0.02	0.708887	0.000008	2.7	0.03	−9.2	0.02	0.491	0.002	123 ± 2
38	Well−Dol	−1.74	0.03	−0.90	0.01			4.3	0.03	−10.7	0.04	0.498	0.002	109 ± 2
39	Tre	−1.78	0.04	−0.93	0.02	0.709539	0.000007	−1.3	0.03	−9.2	0.02	0.506	0.002	102 ± 2
40	IBw	−0.91	0.05	−0.48	0.02	0.708236	0.000008	1.2	0.02	−7.9	0.02	0.471	0.007	139 ± 6
41	IBg	−0.86	0.02	−0.47	0.02			1.1	0.02	−7.4	0.02	0.490	0.007	124 ± 5
42	MVT	−1.96	0.02	−1.02	0.01	0.709427	0.000007	−2.9	0.01	−13.1	0.02	0.428	0.009	180 ± 10
Mean	(±2σ)	−1.44	1.33	−0.75	0.69	0.708928	0.001418	1.8	4.7	−8.6	5.9	0.483		133

* For more details refer to text.

Table 2
Dolomite major and trace element contents combined with X-ray diffraction results, including degree of order (R), CaCO3 content [mol%].

Nr.	Sample	Ca [ppm]	Mg [ppm]	Sr [ppm]	Fe [ppm]	Mn [ppm]	Mg/Ca (moles)	Degree of order	Mol% $CaCO_3$
Marine evaporative dolomite (sabkha)									
1	2a10	253600	101600	168	186	14	0.7	0.36	56.0
2	2a12	245270	113400	165	177	15	0.8		
3	HDK51	218790	131300	104	200	23	1.0	0.66	50.7
4	1b23	218500	128200	109	529	77	1.0	0.53	50.3
5	Bel1a	193000	97060	144	161	46	0.8	0.53	51.0
6	Bel1b	185070	98400	143	414	75	0.9	0.60	51.3
7	Oo	201730	114700	106	799	24	0.9	0.43	51.7
8	Oom	190220	108000	84	987	36	0.9	0.43	51.7
9	Kri	223070	92830	595	2260	85	0.7	0.65	49.9
10	Angola1	179150	106800	20	8078	418	1.0	0.93	48.0
11	B30	118610	71610	65	3497	267	1.0	0.72	50.7
12–14	B31a-c ($n = 3$)	165347	97903	103	2688	195	1.0	0,51	50.6
Mean		194504	104115	147	1811	119	0.9	0.57	51.1
Marine altered ("mixing zone")									
15	Moggast1	217450	128500	49	115	67	1.0	0.93	50.7
16	Hund1	223970	122900	54	677	97	0.9	0.84	50.7
17	Contrin2	218730	127700	26	2038	55	1.0	0.84	51.0
18	Prüstr. 4	215380	131100	7	842	412	1.0	1.00	50.0
Mean		218883	127550	34	918	158	1.0	0.90	50.6
Non-marine evaporative dolomite (Lacustine/palustrine)									
19	Ofeu3	168880	85860	158	2541	1430	0.8	0.67	53.3
20–21	Blei 2a, 2b ($n = 2$)	142210	85260	94	3905	1230	1.0	0.37	50.0
22	StBe20	209600	113700	295	625	40	0.9	0.52	52.0
23–32	Swamp dol ($n = 10$)	203688	87729	81	26523	25777	0.7	0.25	51.7
Mean		181095	93137	157	8399	7119	0.9	0.45	51.8
Hydrothermal dolomite									
33	RSD-Dol	176970	109000	189	254	136	1.0	1.00	50.0
34	5a1	243490	112200	71	143	38	0.8	0.94	50.0
35	5e3	222440	121600	76	149	9	0.9	0.69	50.3
36	Letmathe1	212240	125000	28	4935	1200	1.0	0.94	50.0
37	PH37	220420	122900	28	9293	2480	0.9	0.98	49.3
38	Well-Dol	162830	90020	47	8748	1510	0.9	0.77	49.3
39	Tre	216130	114000	57	14120	1230	0.9	1.00	52.0
40	IBw	218180	124700	61	1391	176	0.9	0.50	50.1
41	IBg	213740	125400	35	406	122	1.0	0.50	50.1
42	MTV	218060	123200	58	3533	349	0.9	0.62	51.1
Mean		210450	116802	65	4297	725	0.9	0.79	50.2

cathodoluminescence colors pointing to a saline environment (cf. Gillhaus et al., 2010). Associated detrital material yields blue to violet cathodoluminescence patterns (Fig. 3F).

Altered marine ($R = 0.90$) dolomite crystals (150–200 μm) consist of euhedral rhombs forming a crystal-supported framework with intercrystalline matrix porosity in an idiotopic mosaic (moldic porosity; Fig. 3C). Relict sediment structures/textures are commonly absent. Relict features of brachiopod shells (sample moggast1; Table 1) and dasycladaceen algae (sample contrin2; Table 1) are visible in thin sections. Crystals have a unimodal size distribution and are typically tan to light grey in transmitted light with moderately abundant fluid inclusions. Individual crystals are characterized by cloudy cores and clear rims with concentric zonation. In the case of the thin sections studied here, cathodoluminescence reveals overall mottled textures with dull to moderate orange-red luminescence colors (Fig. 3D). Mottled, dull red cathodoluminescence patterns are commonly observed in altered dolomites and are often interpreted to be associated with meteoric fluids (Reinhold, 1998) but mottled CL patterns are also known from high-temperature and reflux settings.

The hydrothermal dolomite exhibits much coarser and polymodal grain sizes (>50 μm), relict sedimentary structures/textures or faunal remains are absent, open intercrystalline pore space is more commonly observed, dolomite rhombohedra are planar sub-/euhedral in shape (Füchtbauer and Goldschmidt, 1965; Füchtbauer and Richter, 1988). Hydrothermal dolomites are mainly fabric/structure destructive, formed through recrystallization and/or replacement and consist of coarse crystalline and anhedral crystals with diameters of 200–2000 μm (Fig. 3G). Some are passive precipitates into open

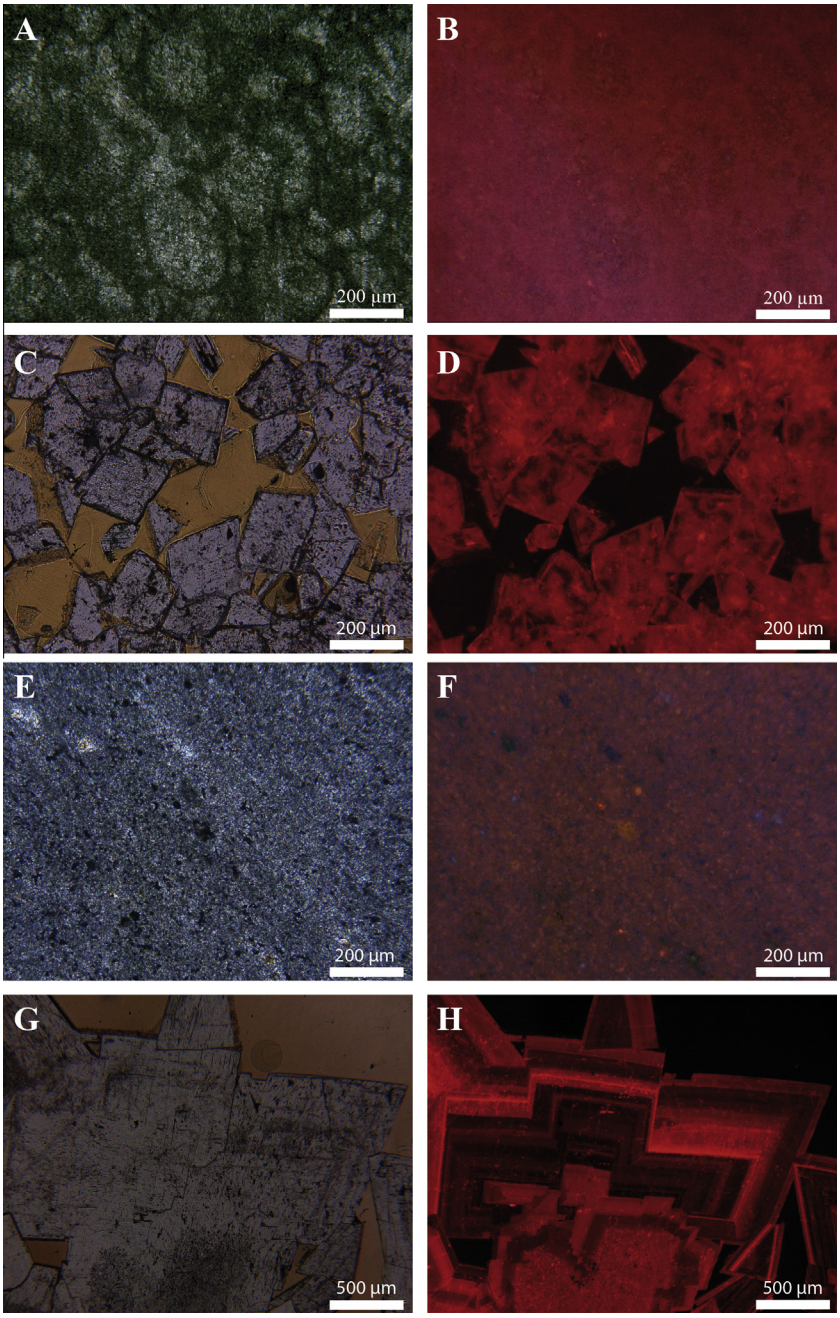

Fig. 3. Photomicrographs of four main dolomite types investigated. (A) Sabkha dolomicrite with pelletal structures under plane polarized light. (B) Dolomicrite displays orange to red cathodoluminescence (A, B: sample HDK2; Triassic (Norian), Central Alps, Austria). (C) Altered marine dolomite characterized by zoned, euhedral rhombs, intercrystalline porosity and moderately abundant inclusions (plane polarized light). (D) The dolomite cement reveals a dull to moderate orange-red cathodoluminescence color (C, D: sample Moggast; Late Jurassic, Franconian Alp, Germany). (E) Laminated lacustrine dolomicrite, precipitated in a saline lake, consisting of microcrystalline anhedral to subhedral crystals (plane polarized light). (F) Cathodoluminescence colors range from yellow to beige. Detrital material is characterized by blue to violet cathodoluminescence (E, F: sample StBe 20; Late Miocene, Steinheim, Swabian Alp, Germany). (G) Hydrothermal saddle dolomites with coarse crystalline, anhedral fabrics. (H) Cathodoluminescence reveals orange-red to dark brown colors and a non-planar to xenotopic mosaic (G, H: sample IB; Late Pennsylvanian, Indian Basin, New Mexico, USA). (For interpretation of the references to color in this figure legend, the reader is referred to the web version of this article.)

pore space. Burial replacement dolomite and saddle dolomite cements are intensely pigmented and display light alternating orange-red to dark brown luminescence colors in a non-planar to xenotopic mosaic (Fig. 3H). Hydrothermal dolomites are characterized by their nearly stoichiometric composition ($R_{burial} = 0.79$).

4.2. Geochemical characterization of dolomites

4.2.1. Magnesium-isotope data

The $\delta^{26}Mg_{dol}$ ratios range between −2.49‰ and −0.45‰ (Table 1 and Fig. 4). The mean $\delta^{26}Mg$ values of the four different dolomite types are: -2.11 ± 0.54‰ (2σ, $n = 14$) for earliest diagenetic sabkha dolomites; -1.41 ± 0.64‰ (2σ, $n = 4$) for altered marine dolomites; -1.25 ± 0.86‰ (2σ, $n = 14$) for earliest diagenetic lacustrine/palustrine (coal ball; Richter et al., 2014) dolomites and -1.44 ± 1.33‰ (2σ, $n = 10$) for hydrothermal dolomites. All dolomite types overlap in their magnesium isotopic composition, with hydrothermal dolomites representing the widest isotope range (±1.33‰ 2σ) observed. The least variable isotope range is present in sabkha dolomite samples (±0.60‰ 2σ). Magnesium-isotope values of Triassic Dolomia Principale sabkha dolomites as reported in Geske et al. (2012; $\delta^{26}Mg_{D2}$ mean: -1.91 ± 0.23‰, $n = 32$), are similar to other sabkha dolomites analyzed in this study (Fig. 4A). A correlation ($R^2 = 0.14$) between $\delta^{26}Mg$ for hydrothermal dolomite and clumped isotope precipitation temperatures is lacking (Fig. 5A).

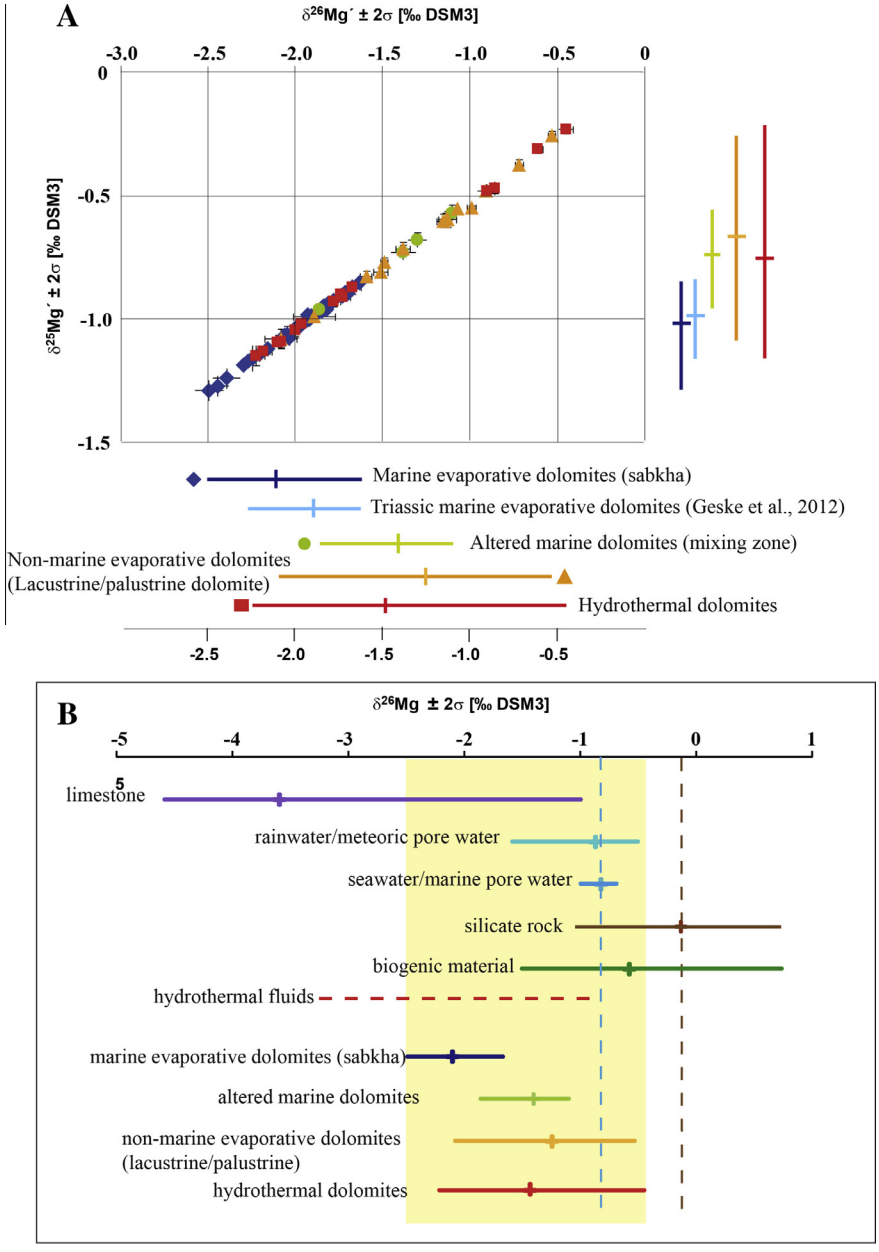

Fig. 4. (A) Three isotope plot illustrating dolomite $\delta^{26}Mg$ for the four main types studied in overview. Magnesium-isotope values range from −2.49‰ and −0.45‰ with an overall mean of -1.75 ± 1.08‰ ($n = 42$). Range of isotope values are shown to the right and beneath the plot for each dolomite type. (B) Magnesium isotopic composition ($\delta^{26}Mg_{DSM3}$) of different Mg sources (limestones, seawater, rainwater, silicate rocks, plant material, are shown for comparison. With decreasing seawater influence, $\delta^{26}Mg$ signatures of sabkha-, mixing zone and lacustrine/palustrine dolomites are increasingly affected by ^{26}Mg-enriched silicate-derived Mg. See text for discussion.

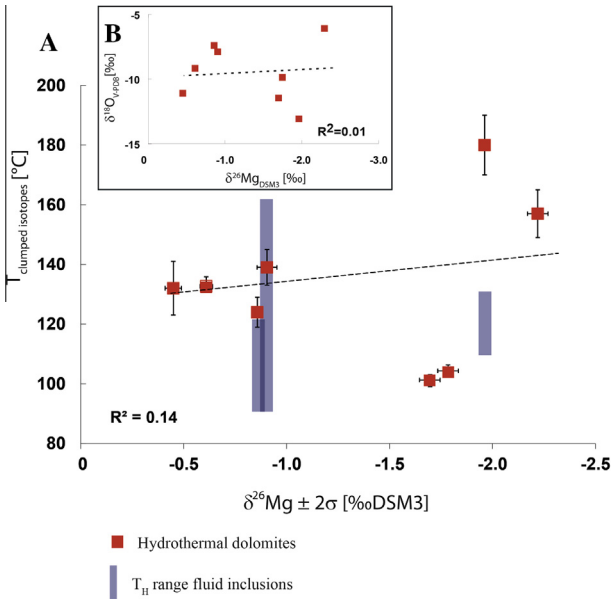

Fig. 5. (A) Hydrothermal dolomite $\delta^{26}Mg$ versus precipitation temperature (°C), as based on the clumped isotope (Δ_{47}) thermometer and Eq. (1). Homogenization temperatures (T_h) based on fluid inclusion analysis (Hiemstra and Goldstein, 2004 and Laskares and Goldstein, written communication) are compared to calculated clumped isotope precipitation temperatures. No correlation ($R^2 = 0.14$) is found between $\delta^{26}Mg$ and fluid temperatures. (B) Inset cross plot documenting poor correlation of magnesium- and oxygen isotope ratios of hydrothermal dolomites ($R^2 = 0.01$).

4.2.2. Supporting geochemical data

Table 1 and Fig. 6 summarize $\delta^{18}O$ and $\delta^{13}C$ isotope ratios of all dolomite types. Mean $\delta^{18}O_{V\text{-}PDB}$ values for altered marine dolomites ($-4.2‰ \pm 1.0$ 2σ, $n = 4$) and earliest diagenetic lacustrine/palustrine dolomites ($-5.3‰ \pm 7.3$ 2σ, $n = 14$) are comparable. Earliest diagenetic sabkha dolomites $\delta^{18}O$ ratios ($-1.4‰ \pm 7.2$ 2σ, $n = 14$) are, in comparison, enriched in ^{18}O. Late diagenetic hydrothermal dolomites yield the isotopically most depleted values ($-8.6‰ \pm 5.9$ 2σ, $n = 10$).

Mean carbon isotopic composition ($\delta^{13}C_{V\text{-}PDB}$) of the earliest diagenetic sabkha dolomites ($+3.1‰ \pm 4.4$ 2σ, $n = 14$), altered marine dolomites ($+2.1‰ \pm 3.6$ 2σ, $n = 4$), and late diagenetic hydrothermal dolomites ($+1.8‰ \pm 4.7$ 2σ, $n = 10$) are similar. The earliest diagenetic lacustrine/palustrine dolomites show distinctly lower $\delta^{13}C$ mean values of $-11.0‰ \pm 12.9$ 2σ ($n = 14$).

Clumped isotope Δ_{47} values for hydrothermal dolomites range from 0.428‰ to 0.506‰ and the corresponding eight calculated precipitation temperatures (Passey and Henkes, 2012) range between 102 and 180 ± 10 °C (Table 1).

Altered marine dolomites are characterized by the lowest $^{87}Sr/^{86}Sr$ ratios (mean = 0.707443, $n = 3$) in comparison to all other dolomite types (Table 1). Strontium-isotope ratios of earliest diagenetic sabkha dolomites (mean = 0.70803, $n = 9$) are similar to those of earliest diagenetic lacustrine/palustrine dolomites (mean = 0.708617, $n = 4$). Late diagenetic hydrothermal dolomites display the most radiogenic strontium isotope ratios (mean = 0.708928, $n = 7$). A weak correlation (linear expression with a stability index of $R^2 = 0.53$) between the strontium isotope and oxygen isotope ratios was observed (Fig. 7). Radiogenic strontium ($^{87}Sr/^{86}Sr$) signatures are correlated to more negative $\delta^{18}O$.

Major and trace elemental abundances are given in Table 2. The strontium concentrations are highest for earliest diagenetic lacustrine/palustrine dolomites

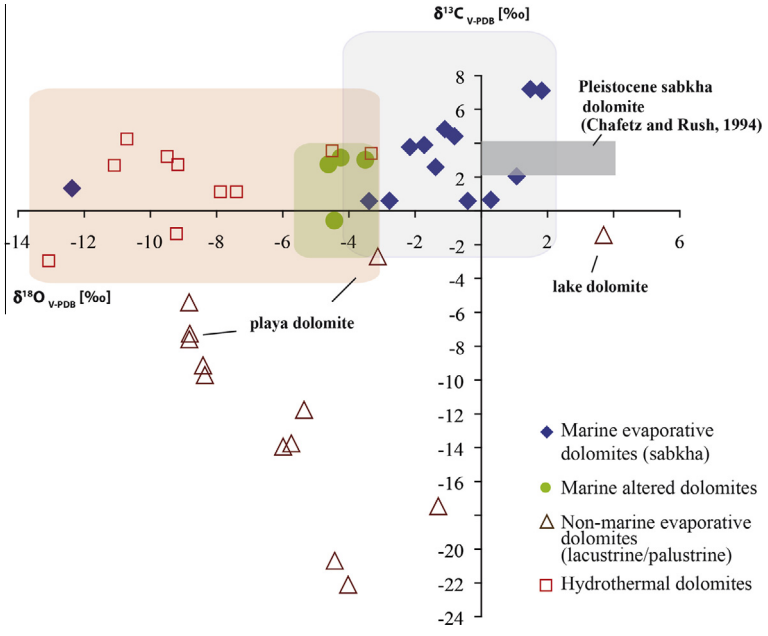

Fig. 6. Oxygen- and carbon isotope ratios of different dolomite types. Dark grey box reflects the range of Pleistocene sabkha dolomites (Chafetz and Rush, 1994). Altered marine dolomites overlap with marine evaporative and hydrothermal dolomites. Lacustrine/palustrine dolomites reveal distinct carbon and oxygen isotopic characteristics.

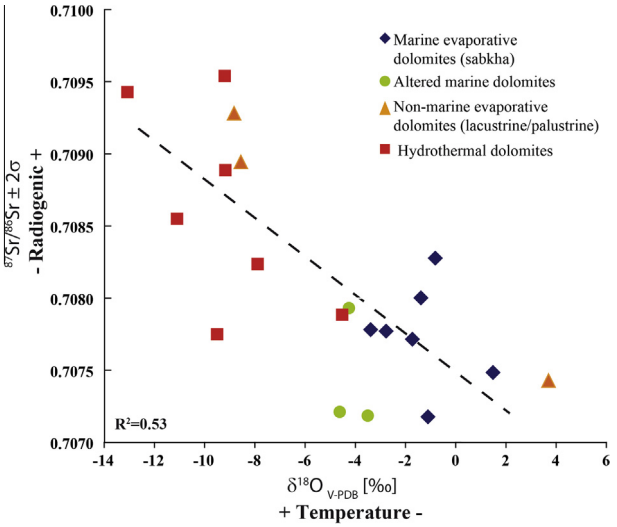

Fig. 7. Oxygen-isotope data plotted against $^{87}Sr/^{86}Sr$ ratios. Dolomite $\delta^{18}O$ ratios decrease with increasing $^{87}Sr/^{86}Sr$ ratios ($R^2 = 0.53$).

($Sr_{mean} = 157$ ppm, $n = 14$), and lowest for altered marine dolomites ($Sr_{mean} = 34$ ppm, $n = 4$). Earliest diagenetic sabkha dolomites are characterized by higher Sr concentrations ($Sr_{mean} = 147$ ppm, $n = 14$) compared to late diagenetic hydrothermal dolomites ($Sr_{mean} = 65$ ppm, $n = 10$). Hydrothermal dolomites, palustrine coal ball dolomites (Torf) and Neoproterozoic sabkha dolomite (Angola1) have the highest Fe and Mn concentrations.

5. INTERPRETATION AND DISCUSSION

5.1. Characterization of dolomite precipitation environments

The type of dolomite relates to its formation (marine, marine evaporative, altered marine, meteoric or hydrothermal) environment. Consequently, any geologically reasonable interpretation of $\delta^{26}Mg_{dol}$ must rest on a solid foundation of the corresponding dolomite precipitation and, where appropriate, diagenetic alteration environment. Particularly, the composition and properties of dolomitization fluids and host rock types (Mg sources), different Mg sinks and stabilization of non-stoichiometric dolomites are crucial for the evolution of natural dolomites. Using well constrained reference dolomite samples and their geochemical, mineralogical and crystallographic properties as a starting point, we here briefly document the main properties of the dolomitization environments relevant to this study.

5.1.1. Marine evaporative dolomites (sabkha)

Marine evaporative dolomites precipitate from low temperature marine porewaters characterized by high salinities (50–90 g/l; Lokier and Steuber, 2009). Temperatures in modern pore-fluids in the coastal sabkha of Abu Dhabi range between 20 °C in winter and 40 °C in summer (Lokier et al., 2013). Sabkha dolomites analyzed in this study yield $\delta^{18}O_{sabkha\text{-}dol}$ values of −1.4‰. Applying the equation of Vasconcelos et al. (2005), calculated temperatures with fluid values of +3.5‰ [SMOW] indicate precipitation of dolomicrites from fluids with a mean annual surficial pore fluid temperature of around 20 °C. The poorly ordered and Ca-rich crystal lattice of most marine evaporative dolomites (degree of order $(R)_{sabkha} = I\ d_{(110)}/d_{(015)}$=0.6) and their microscopic textures, composed of homogenous crypto- to microcrystalline anhedral to subhedral crystal rhombs, are in many cases evidence of a low degree of recrystallization implying good preservation (Fig. 3A, B, E, F; Radke and Mathis, 1980; Gregg and Sibley, 1984; Sibley and Gregg, 1987). The same conclusion is also drawn from dolomite $^{87}Sr/^{87}Sr_{mean}$ ratio of 0.70809 (Fig. 7 and Table 1) that is similar to recent sabkha pore fluids (Müller et al., 1990). In addition, these dolomites contain on average 147 ppm of Sr (Table 2) and thus fall in the expected Sr value (<300 ppm) of dolomites that precipitated from seawater or evaporated seawater (Land, 1980; Machel and Anderson, 1989; Vahrenkamp and Swart, 1990; Banner, 1995; Budd, 1997; Swart et al., 2005; Suzuki et al., 2006). Finally, the mean $\delta^{13}C$ values of sabkha dolomites (+3.1‰) indicate a marine carbon source, reflecting the carbon isotopic composition of modern carbonate platform sediments (Lowenstam and Epstein, 1957; Milliman, 1974; McKenzie, 1981). Note, in some cases, however, clear evidence for meteoric alteration has been reported (Chafetz and Rush, 1994) and generalized statement regarding the preservation of marine evaporative dolomites should be avoided.

5.1.2. Altered marine dolomites

Altered marine dolomites (often an admixture of marine and evaporated marine low temperature dolomite) are precipitated from seawater with ambient (low) temperatures and subsequently were overprinted in the presence of non-marine fluids (Machel, 2013). The salinity of the dolomitizing fluids is lower, compared to those of sabkha dolomite formation environments (<35–36 g/l). Altered marine dolomites (degree of order = 0.9) were partly recrystallized probably at low temperatures as evident from cathodoluminescence analysis (Fig. 4C, D). These dolomites reflect the $^{87}Sr/^{86}Sr$ isotope ratios (0.7074) of the diagenetic fluids. In addition, lower Sr contents of 34 ppm, due to lower Sr/Ca ratios of the solution, result from mixing of calcium-rich fluids with seawater (Swart et al., 2005). Mean $\delta^{13}C$ values of altered marine dolomites (+2.1‰) indicate a marine carbon source, reflecting the carbon isotopic composition of modern carbonate platform sediments (Lowenstam and Epstein, 1957; Milliman, 1974; McKenzie, 1981). In the case of altered marine dolomites, oxygen isotope values are often depleted ($\delta^{18}O_{V\text{-}PDBmean} = -4.2‰$) relative to those from sabkha environments and point to meteoric diagenetic alteration. In addition, partial recrystallization leads to larger average crystal diameters (Fig. 4C, D, G, H; Land, 1980).

5.1.3. Non-marine, evaporative dolomite (saline palustrine/lacustrine)

Lacustrine (lake) and palustrine (swamp; coal balls see discussion in Richter et al., 2014) dolomites are characterized by precipitation from highly saline pore fluids (saline

lakes, playas; De Deckker and Last, 1988; Last et al., 2010, 2012) in a low temperature regime. The assignment of dolomites to this depositional environment is evident from (i) petrographic and (ii) geochemical data in combination with (iii) stratigraphic and palaeo-geographic evidence. Lacustrine/palustrine dolomites analyzed here yield $^{87}Sr/^{86}Sr$ ratios of 0.707–0.709 (Table 1 and Fig. 7). These values are comparable to $^{87}Sr/^{86}Sr$ ratios of lake dolomites (0.709–0.715; Faure and Powell, 1972). The radiogenic strontium isotopic composition of these dolomites reflects an admixture of different sources including variable hinterland and host rock lithologies.

Dolomites in lacustrine sediments are commonly characterized by strontium contents of about 100 ppm (M'Rabet, 1981). Lacustrine/palustrine dolomites analyzed in the context of this study contain, on average, 157 ppm Sr (Table 2) a value that agrees with the predicted Sr elemental range (100–300 ppm). Mean $\delta^{13}C$ value of lacustrine/palustrine dolomites (−6.3‰), and particularly of swamp dolomites (−13.5‰; Fig. 6), represent the most depleted carbon isotopic ratios of all dolomites investigated in this study. This pattern suggests the influence of light carbon organic matter and from bacterial oxidation/sulfate reduction (Irwin et al., 1977; Machel et al., 1995) or soil-zone CO_2 ($\delta^{13}C_{soil\text{-}zone\ CO2}$: −12‰ to −20‰; Cerling and Quade, 1993).

5.1.4. Hydrothermal dolomites

Hydrothermal dolomites, especially those associated with Mississippi Valley-type (MVT) deposits and samples from the Indian Basin in New Mexico (USA), are precipitated from warm to hot, highly saline, basement-derived brines (salinity of up to 23w% NaCl equivalent; Kesler et al., 1996). The origin of hydrothermal dolomites analyzed in the context of this study is evaluated by (i) petrographic properties typical for burial/hydrothermal (saddle) dolomites; (ii) fluid inclusion studies; (iii) clumped isotope palaeo-thermometry and (iv) carbon, oxygen and strontium isotope data. Published fluid inclusion data (Hiemstra and Goldstein, 2004, 2014), pointing to precipitation/recrystallization fluid temperatures on the order of 90–170 °C and reasonably agree with clumped isotope data pointing to temperatures of 120–180 °C as shown here. Additional information comes from the Saddle dolomite petrography of these carbonates indicating precipitation temperatures of above 60 °C (Sibley and Gregg, 1987; Fig. 4G, H).

The $^{87}Sr/^{86}Sr_{mean}$ ratio of 0.7089 (Fig. 7 and Table 1) is attributed to advection and concomitant interaction with siliciclastic rocks (breakdown of detrital feldspars, alteration of clay minerals; Chaudhuri and Clauer, 1993; Malone et al., 1996; Davies and Smith, 2006). Strontium isotope ratios of basinal brines are enriched in ^{87}Sr and $^{87}Sr/^{86}Sr$ of above 0.708 are found (Spötl and Pitman, 1998). These dolomites lost some of their former Sr during burial diagenesis via diffusion and precipitation/dissolution processes (Frisia, 1994). In analogy to this, hydrothermal dolomites contain low Sr_{mean} values of 65 ppm (Table 2).

Decreasing $\delta^{18}O$ values correlated to increasing $^{87}Sr/^{86}Sr$ ratios ($R^2 = 0.53$) are a typical feature of hydrothermal dolomite samples reported here (Fig. 7). This pattern is attributed to the alteration of low-temperature dolomite under the influence of warm to hot fluids. Elevated subsurface temperatures lead to a significant depletion of the $\delta^{18}O$ values of these early diagenetic, metastable Ca-rich dolomites ($\delta^{18}O_{mean} = -8.6‰$; Mattes and Mountjoy, 1980; Cander et al., 1988; Wallace, 1990; Jaffrés et al., 2007). The equation of Matthews and Katz (1977) is applied to the hydrothermal dolomite $\delta^{18}O$ data ($\delta^{18}O_{mean} = -8.6‰$) as compiled here:

$$1000 \ln \alpha_{Dol-H2O} = 3.06 * 10^6 T^{-2} - 3.24 \quad (3)$$

Assuming that these dolomites were formed from dolomitization fluids at elevated temperatures as calculated from $T(\Delta_{47})$ [120–180 °C], calculated $\delta^{18}O_{fluid}$ values were found to range between +4‰ and +14‰ VSMOW. Regarding the samples from the Indian Basin, New Mexico (USA) these calculated fluid oxygen isotope composition point to mixture between a highly saline (oil-field) brines and brines associated with evaporates (Hill, 1996).

5.2. Dolomite Mg isotope signatures

Dolomites documented in this study display a wide range of $\delta^{26}Mg$ values, ranging from −2.49‰ to −0.45‰ ($\delta^{26}Mg_{mean} = -1.75 \pm 1.08‰$, $n = 42$), and are in agreement with "dolomite Mg isotope data" *sensu lato* as reported in previous studies ($\delta^{26}Mg_{mean}$ of $-1.76 \pm 0.77‰$ ($n = 124$); Fig. 8, Table 3; Galy et al., 2002; Chang et al., 2003; Tipper et al., 2006a, 2008a,b; Brenot et al., 2008; Wombacher et al., 2009; Jacobson et al., 2010; Higgins and Schrag, 2010; Pokrovsky et al., 2011; Geske et al., 2012; Azmy et al., 2013; Mavromatis et al., 2014; Fantle and Higgins, 2014). Magnesium isotope data of all investigated dolomite types in this study show similar average $\delta^{26}Mg$ values of −2.11‰ (±0.54‰ 2σ; $n = 14$, marine evaporative), −1.41‰ (±0.64‰ 2σ; $n = 4$, altered marine), −1.25‰ (± 0.86‰ 2σ, $n = 14$, lacustrine/palustrine) and −1.44‰ (±1.33‰ 2σ, $n = 10$, hydrothermal) (Fig. 4).

The main source of Mg for recent sabkha type dolomite (mean value of $-2.11‰ \pm 0.54‰$ 2σ; $n = 14$) precipitation is evaporated marine pore fluid (mean $\delta^{26}Mg_{seawater} = -0.82‰$, see also Foster et al., 2010; Ling et al., 2011, and references therein). In many cases, however, the non-stoichiometric, microbially induced sabkha dolomites, may stabilize after deposition to (more) stoichiometric phases through a dissolution/re-precipitation process occurring at an early diagenetic stage and therefore may reflect the Mg isotope composition of the, somewhat isotopically altered, pore fluid (McKenzie, 1981; Van Lith et al., 2003b; Dupraz et al., 2009; Roberts et al., 2013; Paulo and Dittrich, 2013). Work by these authors commonly suggests that Mg ions are complexed and de-hydrated by surface-bound carboxyl groups and thus a decreased amount of energy is required for carbonation. Nevertheless, Mavromatis et al. (2012) and Shirokova et al. (2013) suggested that microbial activity does not appreciably affect the Mg isotope fractionation factors in the hydrous Mg-carbonate-fluid system. Earliest diagenetic stoichiometric dolomite $\delta^{26}Mg$ signatures in recent sabkha environments

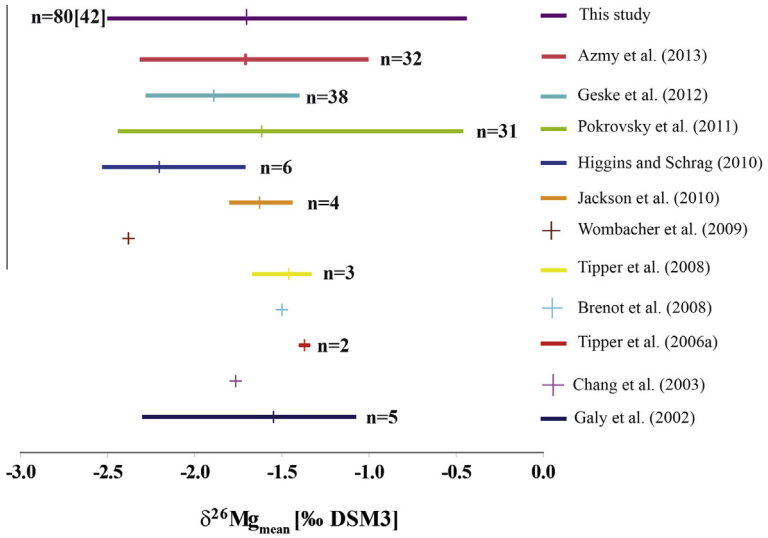

Fig. 8. Comparison of δ^{26}Mg data range shown here with those from various published sources. Most authors do not specify the dolomite types analyzed (Table 3). Dolomite magnesium isotopic ratios documented in this study cover the full range of all previously reported dolomite data.

Table 3
Compilation of published dolomite Mg isotope data.

Reference	Min δ^{26}Mg [‰ DSM3]	Max δ^{26}Mg [‰ DSM3]	Mean δ^{26}Mg ± 2σ [‰ DSM3]	*n*	Dolomite type
This study	−2.49	−0.45	−1.75 ± 1.08	42	Sabkha, palustrine/lacustrine mixing, hydrothermal
Galy et al. (2002)	−2.29	−1.09	−1.55 ± 0.92	5	Unspecified
Chang et al. (2003)	−1.77	−1.77	−1.77 ± 0.04	1	Unspecified
Tipper et al. (2006a,b,c)	−1.39	−1.35	−1.37 ± 0.06	2	Unspecified
Brenot et al. (2008)	−1.50	−1.50	−1.50 ± 0.20	1	Unspecified
Tipper et al. (2008a,b)	−1.39	−1.35	−1.37 ± 0.06	2	Unspecified
Wombacher et al. (2009)	−2.38	−2.38	−2.38 ± 0.18	1	Unspecified
Jacobson et al. (2010)	−1.79	−1.45	−1.63 ± 0.35	4	Sabkha?
Higgins and Schrag (2010)	−2.52	−1.72	−2.20 ± 0.64	6	Organogenic dolomite, deep sea
Pokrovsky et al. (2011)	−2.43	−0.47	−1.61 ± 0.98	31	Sabkha, mixing, unspecified
Geske et al. (2012)	−2.27	−1.41	−1.89 ± 0.33	38	Sabkha
Azmy et al. (2013)	−2.27	−1.00	−1.75 ± 0.60	32	D1 shallow water, D2 + D3 burial?

in Abu Dhabi range from −0.5‰ to −1.1‰. Our present understanding is that the variable magnesium isotope signature of sub-recent sabkha dolomites is related to complex kinetics of precursor formation, dissolution/precipitation reactions including microbiological effects and involves variable Mg sources and sinks in a temporally and spatially variable microenvironment.

The observation that fossil sabkha dolomites from different time intervals (Neoproterozoic, Mississippian, Permian, Triassic and Pleistocene) display more negative mean δ^{26}Mg ratios (−2.11‰ ± 0.54‰ 2σ; $n = 14$; Fig. 4) than those from modern systems (−0.5‰ to −1.1‰) merits attention. It could be hypothesized that this is because of secular changes controlled by plate tectonic configuration and continental runoff (Tipper et al., 2006b; Wimpenny et al., 2014b), changes in seawater Mg/Ca ratio and evolutionary trends of marine organisms (Stanley, 2006) sea-level change and related waxing and waning of epeiric seas affecting carbonate precipitation and dissolution as well as changes in seafloor spreading rates and oceanic hydrothermal activity (Tipper et al., 2006c; Beinlich et al., 2014). All are expected to affect $\delta^{26}Mg_{seawater}$ ratios on the time scale of many Myr (Pogge von Strandmann et al., 2014). Modern seawater δ^{26}Mg values are on the order of −0.82‰ independent of water depth or geographic location (see references in Hippler et al., 2009). Its secular variation is expected to vary only slowly due to long $Mg_{seawater}$ residence times of $\tau \sim 13$ Myr were suggested by Broecker and Peng (1982) and the variables discussed above. At present, however, the only study assessing possible temporal changes in seawater δ^{26}Mg is the one by Higgins and Schrag (2012) showing downcore fluctuations in bulk sediment δ^{26}Mg in excess of 1.5‰ attributed to a secular range of seawater Mg over the Neogene. Such secular changes,

however, cannot be the only explanation for the differences between modern sabkha dolomite $\delta^{26}Mg$ and that of the ancient. The ancient values range between −2.49‰ and −1.67‰, i.e. less than 1‰. The youngest of the ancient samples is a Pleistocene one from Abu Dhabi, with $\delta^{26}Mg$ of −2.05, essentially a sample from northern Gulf in Saudi Arabia close to the modern sabkha samples, just slightly older. This value is 1‰ more negative than the most negative of the modern samples. Because of the young age, this shift cannot be explained by secular variation, and thus, their compositions must be explained by alteration of the original dolomite. In a recent paper, Pogge von Strandmann et al. (2014) present an interpretation of $\delta^{26}Mg_{seawater}$ over the last 40 Myr as based on foraminifera tests. Assuming that these data are valid, $\delta^{26}Mg_{seawater}$ gradually shifts from the present value of −0.82 to values near 0‰ at 20 Ma. Given that the reported shift to less negative seawater values is the opposite of what we observed in the Pleistocene sabkha dolomites, that are more negative in terms of their $\delta^{26}Mg$ isotope ratios relative to recent ones, we conclude that it is likely that $\delta^{26}Mg$ values of the ancient sabkha dolomites have been diagenetically reset. Their compositions are likely controlled by a combination of the original setting, diagenetic alteration and secular variation of the system, and thus, compositions do not lie in a clearcut and distinct $\delta^{26}Mg$ field compared to other dolomites.

Altered marine dolomites yield $\delta^{26}Mg$ ratios of −1.86‰ to −1.10‰ with a mean of -1.41 ± 0.64‰ ($n = 4$). Altered marine dolomite $\delta^{26}Mg$ values are mostly less negative than those of sabkha dolomites and similar to those of lacustrine/palustrine and hydrothermal dolomites (Fig. 5; Table 1). This dolomite type is characterized by intercrystalline vuggy and moldic porosity and consists of zoned crystals (Fig. 4C, D) similar to hydrothermal dolomites. These dolomites are expected to reflect a mixed low-temperature Mg source (<30 °C) including seawater Mg and also Mg derived from diagenetic fluids (Fig. 4B). As the case for all carbonate $\delta^{26}Mg$ signatures, non-equilibrium fractionation factors between low temperature fluid and dolomite (Schauble, 2011) as well as possible Mg sinks during dolomite precipitation (Wimpenny et al., 2014a) are considered to play a significant role.

The $\delta^{26}Mg$ values of lacustrine and palustrine dolomites range between −2.08‰ and −0.53‰ with a mean of -1.25 ± 0.86‰ (2σ, $n = 14$). These dolomites precipitate in the context of marine transgressions over low-lying coastal swamp areas (Fig. 2; Richter et al., 2014, and references therein) or in hypersaline lakes. The main Mg source is seawater percolating downwards into organic-rich swamp deposits during marine transgressions in the case of palustrine dolomites. In the case of lacustrine dolomites, the main Mg source is saline continental groundwater. As for sabkha-type dolomites, the evaporated pore fluid $\delta^{26}Mg$ signature might have changed over time. Lacustrine and palustrine dolomites precipitate in organic-rich host sediments that contain abundant Mg-bearing silicates and plant material. Similar to continental weathering pathways (Riechelmann et al., 2009, 2012a), it seems likely that Mg bearing silicates contributed magnesium with an isotope ratio in the order of about −0.2‰ to the dolomite crystals during precipitation and diagenetic processes (Higgins and Schrag, 2012; Fig. 4B) but the co-precipitation of Mg-bearing sheet silicates (Wimpenny et al., 2014a) is also expected to affect $\delta^{26}Mg_{fluid}$. There is evidence to suggest that silicates might preferentially release ^{24}Mg into the pore fluid during leaching and dissolution but the related processes are insufficiently understood. Moreover, if secondary silicates form in the weathering domain, these preferentially uptake isotopically heavy Mg leaving the pore fluid depleted (Wimpenny et al., 2014a). Moreover, the influence of plant or microbial soil activity will further affect both products and processes (Bolou-Bi et al., 2010). Precipitation temperatures are poorly constrained and may vary significantly between different precipitation environments but remain in the range of ambient land surface temperatures for tropical to sub-tropical environments to arid regions.

Late diagenetic hydrothermal dolomites display the most diverse $\delta^{26}Mg$ range of −0.45‰ to −2.22‰ and are characterized by mean values of −1.44‰ (±1.33‰ 2σ, $n = 10$; 5A, B, Table 1). Dolomite precipitation in the burial realm differs from all other dolomitization environments discussed here due to the elevated fluid temperatures of 90–180 °C as deduced from clumped isotope and fluid inclusion data. At such high temperatures, dolomite formation and the rate of dolomitization is influenced by several factors including solution Mg/Ca ratio and degree of fluid supersaturation with respect to dolomite (Sibley et al., 1994). Moreover, the burial domain is rock dominated with respect to Mg sources for the dolomitizing fluids. Saddle dolomites from the Indian Basin in New Mexico (USA), for example, were associated with hydrothermal fluid flow driven by thermal convection following tectonic fracturing (Hiemstra and Goldstein, 2004, 2014). Evidence for hydrothermal fluid flow includes fluid inclusion data, with typical repeated rise and fall in fluid temperature (90–160 °C; Hiemstra and Goldstein, 2004), and a spatial distribution of Sr isotopes and oxygen isotopes indicating preferred fluid flow and highest temperatures in fault damage zones.

Hydrothermal fluids sampled in the Atlantic/Pacific domain are found to be either “indistinguishable” from seawater or enriched in ^{24}Mg by up to 2.4‰ relative to seawater (Galy et al., 2006; Fig. 4B). The broad magnesium isotope data scatter of hydrothermal dolomites (±1.33‰, 2σ) and the often complicated zonation of hydrothermal dolomites including precipitation and dissolution features is in agreement with a multi-source origin of Mg and its changes with time (Fig. 3G, H). Given that aquifer bulk geochemistry (source), rock–water interaction, fluid chemistry and properties as well as Mg sinks differ spatially and temporally within individual basins and between different basins, the resulting scatter in hydrothermal fluid $\delta^{26}Mg$ ratios is not surprising. In contrast to the previously reported low-temperature settings, kinetic factors related to the dehydration of Mg aquo-complexes are expectedly less significant at elevated temperatures (Pearce et al., 2012). Conversely, dolomite precipitation rates are expected to be higher at elevated temperatures whereas the influence of precipitation rates on carbonate $\delta^{26}Mg$ ratios may be subdued and the actual $\delta^{26}Mg_{dol}$ to reflect near isotope

equilibrium conditions (Pearce et al., 2012; Beinlich et al., 2014).

Clumped isotope thermometry allows new insights into both the temperature and the source of diagenetic fluids recorded in ancient carbonates (Ferry et al., 2011). As a first step, the possibility of a re-equilibration/resetting of hydrothermal dolomites during deeper burial/recrystallization with regard to clumped isotopes and Mg isotopes must be considered. Diffusional blocking temperatures for slowly cooled regional metamorphic dolomite marbles are found to be around 300 °C (Eiler, 2011). First partial re-equilibration is proposed for temperatures greater than 250 °C (calcite; Dennis et al., 2011). The clumped isotope temperatures of various dolomites are well below these blocking temperatures (120–180 °C). When plotting $\delta^{26}Mg_{dol}$ against fluid temperatures as deduced from clumped isotope data in this study (Fig. 5) no obvious relation is found ($R^2 = 0.14$). These findings agree with previous work (Geske et al., 2012; Lavoie et al., 2014; Li et al., 2014a,b) suggesting that temperature-induced, $\Delta^{26}Mg_{fluid\text{-}dol}$ sensu Schauble (2011) is blurred and overprinted by factors such as kinetics, Rayleigh fractionation or changes in the sources and sinks of Mg in the fluid over time. The fact that here, hydrothermal dolomites from several basins are merged into one data set complicates the issue. The way forward is clearly the combination of fluid inclusion and clumped isotope thermometers applied to well-constrained dolomite samples from one basin.

5.3. Fluid versus rock dominated dolomitization environments

The main source of Mg for marine or lacustrine dolomites, derived from the (dolomitizing) pore fluid, is sea or lake water and, in the absence of secondary diagenetic resetting, changes in $\delta^{26}Mg_{porewater}$ could be expected to be recorded in ancient marine (or lacustrine) dolomites (Higgins and Schrag, 2012). Commonly, the volume of sea or lake water by far exceeds the volume of the marine dolomites formed. Considering cool to moderately warm fluid temperatures (<60 °C; sabkha type dolomites, altered marine dolomites and lacustrine/palustrine dolomites), the activation energy for dolomite precipitation is high and here, dehydration of free Mg aquo ions is arguably one of the most important parameters controlling dolomite $\Delta^{26}Mg_{fluid\text{-}dol}$ (Mavromatis et al., 2013; Li et al., 2014a,b). As detailed in Li et al. (2014a,b), the average bond lengths for Mg in different carbonate minerals where Mg is a constituent are additional and important factors affecting the fractionation between fluid and different carbonate minerals. Nevertheless, given that we here refer to dolomites only, mineralogical differences in bond lengths seem less important.

Conversely, in the basinal (burial) domain, rock–water interaction under elevated fluid temperatures and corresponding sources and sinks of magnesium are dominant factors affecting $\delta^{26}Mg_{dol}$ (Geske et al., 2012; Azmy et al., 2013; Lavoie et al., 2014). Whilst the temperature related fractionation kinetics for dolomite is not constrained, a number of general considerations offer themselves. The reactivity between a solid and a solution percolating through a given lithology depends mainly on the saturation state of the pore fluid with respect to the minerals present and results in changes of the solid and the solution composition (Morse and Arvidson, 2002; Bjorlykke and Jahren, 2012). Moreover, there is evidence that at equilibrium, there is chemical and isotopic exchange in fluid-rock systems (Pearce et al., 2012). Commonly, high-temperature basinal brines have experienced significant rock–water interaction. Inorganic magnesium sources during diagenesis include the pore fluid, dissolved or leached Mg derived from carbonate rocks (limestone, dolostone, marble; Immenhauser et al., 2010), evaporites, silicate rocks such as basalts, granites, saprolites, diabase, sandstones or loess (Wimpenny et al., 2014a, and references therein), ultramafics (Beinlich et al., 2014) and metamorphic (Li et al. (2014a,b)) or volcanic rocks (Pogge von Strandmann et al., 2008a,b; Opfergelt et al., 2012). Obviously, as documented by the often zoned nature of hydrothermal dolomites (Fig. 3H), burial fluids change with respect to their properties through time. Magnesium sinks that affect the $\delta^{26}Mg_{fluid}$ include diagenetic carbonates precipitated in the aquifer or along faults prior to reaching the dolomitization site (prior calcite precipitation sensu Wassenburg et al., 2013) and secondary clay minerals (Higgins and Schrag, 2010; Wimpenny et al., 2014a) representing a sink for the free Mg aquo ion.

In conclusion, lacustrine or marine dolomitization environments differ in several respects from those of the burial realm, whilst fundamental dolomite precipitation kinetics will remain generally applicable. Perhaps most important is the dominance of sea- or lake water, representing the main Mg source in these dolomitization environments, that in the subsurface, is contrasted by the elevated temperature and different chemistry of burial brines dominated by rock–water interaction. Specifically, in burial environments, it is often the host rock and related leaching and dissolution processes that affect or even control the pore fluid chemistry. Moreover, ancient marine dolomites undergo, in many cases, differential burial-diagenetic pathways leading to the precipitation of late dolomite cements in pore space. When sampled without control on the petrography of these rocks, an unspecified admixture of environmental and diagenetic phases and signals results.

5.4. Open versus closed system behavior

Rock buffered, “closed” diagenetic systems refer to environments where pore waters are subject to multiple dissolution-precipitation cycles within one rock type (Lohmann, 1978; Czerniakowski et al., 1984; Melim et al., 2002; Bjorlykke and Jahren, 2012; Geske et al., 2012). Along with these solution-precipitation cycles, the pore water composition is progressively modified (Morse and Arvidson, 2002). In a “closed” system all available pore space is filled with a diagenetic fluid that exchanges its geochemical composition with the host mineral phase and thus approaches geochemical/isotopic equilibrium. Having said this, the authors acknowledge that the term “closed system behaviour” is at best conceptual. This is because geochemically fully closed environments are unlikely to exist in natural systems.

With regards to the Mg isotope system of dolomites, an example of a "closed" diagenetic, rock buffered system was described for the Norian Dolomia Principale (Hauptdolomit) in the Alpine realm (Geske et al., 2012). The burial Mg source was dominated by Mg recycled from the Dolomia Principale sabkha dolomite itself. Here fluids circulated in a regionally extensive and stratigraphically very thick dolostone rock body with limited internal geochemical ($\delta^{26}Mg$) variability. The Dolomia Principale $\delta^{26}Mg$ isotope ratios remain invariant above 100 °C ($\delta^{26}Mg_{D2}$ mean [100 °C] = $-1.84 \pm 0.16‰$, $n = 8$; $\delta^{26}Mg_{D2}$ mean [350 °C] = $-1.89 \pm 0.13‰$, $n = 7$). Apparently, the observed burial homogenization of $\delta^{26}Mg$ ratios under increasing temperature leads to increasing rates of rock–water interaction (Morse and Arvidson, 2002; Watson and Baxter, 2007).

Conversely, Mississippi Valley type samples (Table 1, Appendix A1) are all hydrothermal in origin. Fluid inclusions from these and other hydrothermal dolomites reveal homogenization temperatures (T_h) of 90–170 °C (Hiemstra and Goldstein, 2004), a range that is in good agreement with calculated precipitation temperatures estimated from clumped isotope thermometry (102–180 °C; Table 1 and Fig. 5a). From the conceptual perspective taken here, we consider Mississippi Valley type and other hydrothermal dolomites as open system precipitates, but derived from basinal brines that have undergone extensive rock–water interaction. The $\delta^{26}Mg_{calcite\text{-}solid}$ fractionation matches that expected for an equilibrium relation (Li et al., 2012a), where fractionation in crystalline materials and solutions decrease with increasing temperature (Fig. 5A; Schauble, 2004).

Concluding, the issue of open versus closed diagenetic environments requires attention when dealing with ancient dolostones. Essentially, previous work has shown that dolomite $\delta^{26}Mg$ ratios from subsamples taken in a volumetrically large dolostone rock body show remarkably conservative (closed system) behavior even when exposed to burial diagenesis reaching fluid temperatures of 350 °C. This is promising with regard to for example Precambrian dolostone successions. Conversely, stratigraphically thin or spatially limited dolostone rocks bodies may undergo significant geochemical alteration in an open system diagenetic setting even when exposed to limited burial depths and temperatures.

6. CONCLUSIONS

A total of 42 samples of four different types of Precambrian to Phanerozoic dolomites (sabkha; altered marine (formerly "mixing zone"); lacustrine and palustrine; hydrothermal) were investigated for their corresponding magnesium-isotope signatures. Precipitation and subsequent diagenetic pathways of all analyzed samples were established, unless well documented in previous work, by means of supporting sedimentological, petrographic, crystallographic and circumstantial geochemical evidence. Magnesium isotope data of all investigated dolomite types in this study show the following average $\delta^{26}Mg$ values: $-2.11‰$ ($\pm 0.54‰$ 2σ; $n = 14$, marine evaporative sabkha), $-1.41‰$ ($\pm 0.64‰$ 2σ; $n = 4$, altered marine, formerly "mixing zone"), $-1.25‰$ ($\pm 0.86‰$ 2σ, $n = 14$, lacustrine/palustrine) and $-1.44‰$ ($\pm 1.33‰$ 2σ, $n = 10$, hydrothermal). This implies that dolomites lack typical $\delta^{26}Mg$ signatures characterizing their specific environment of dolomitization precipitation.

Early diagenetic sabkha dolomites are characterized by the most depleted $\delta^{26}Mg$ signatures of $-2.11 \pm 0.54‰$ (2σ, $n = 14$). Precipitating pore fluids reach temperatures on the order of 20–30 °C. The main Mg sources include seawater and pre-existing metastable carbonate minerals. Variation is in part reflective of original diagenetic setting, later alteration and secular variation.

Stoichiometric altered marine dolomites yield marine Sr isotope values (0.7074), whereas C (2.1‰) and O (−4.2‰) isotope values point to significant alteration. The $\delta^{26}Mg_{mean}$ ratios of altered marine dolomites are $-1.41 \pm 0.64‰$ (2σ, $n = 4$) and are not distinctly different from lacustrine/palustrine dolomites or hydrothermal dolomites, but may be slightly enriched in relation to sabkha dolomites.

Early diagenetic disordered lacustrine and palustrine dolomite Sr isotope ratios (0.7085) and $\delta^{13}C$ isotope signatures (−6.3‰) point to a silicate Sr source and bacterial oxidation during dolomitization. The $\delta^{26}Mg_{mean}$ values of lacustrine and palustrine dolomites are $-1.25 \pm 0.86‰$ (2σ, $n = 14$) implying that these dolomites may be slightly enriched in ^{26}Mg compared to those of sabkha environments.

Late diagenetic (stoichiometric) hydrothermal dolomites yield radiogenic $^{86}Sr/^{87}Sr$ ratios (0.7089) pointing to precipitation from dolomitization fluids characterized by radiogenic Sr signatures. Clumped isotope fluid temperatures are above 120 °C (Δ_{47}) for zoned dolomite crystals but lack a systematic relation to $\delta^{26}Mg_{dol}$. Hydrothermal dolomites display relatively heavy $\delta^{26}Mg$ signatures and display the widest range in dolomite $\delta^{26}Mg$ ratios (mean of $-1.44‰$; $\pm 1.33‰$, $n = 10$). Multiple and temporally changing carbonate–silicate Mg sources, variable fluid reservoirs and fractionation effects provide reasonable explanations for the observed scatter in $\delta^{26}Mg$ ratios.

The present paper provides a foundation for future research and offers a wealth of background required to interpret dolomite $\delta^{26}Mg$ ratios in their depositional and diagenetic framework. The present knowledge on dolomite fractionation factors is discussed and placed in context with the data shown here. Based on this work, it is concluded that the compilation of insufficiently constrained, bulk-dolomite data sets and particularly the extraction of sophisticated interpretations from these data sets with respect to changes in dolomite formation environments or seawater geochemistry can lead to erroneous conclusions. Nevertheless, it is also suggested that dolomite $\delta^{26}Mg$ can in principle be interpreted when placed within a sufficiently detailed framework of understanding.

ACKNOWLEDGEMENTS

The technical staff at Bochum is greatly acknowledged for their support in the (non-)traditional isotope and the cathode luminescence laboratory. The German Science Foundation (grant IM 44/

7-1) is acknowledged for financial support. H.S. Chafetz is acknowledged to provide Pleistocene sabkha dolomite samples for this study. The authors acknowledge critical comments by M. Dietzel and GCA reviewers E. Tipper, J. Wimpenny, P. Pogge von Strandmann and an anonymous referee as well as the editorial handling by A. Jacobson.

APPENDIX A. SUPPLEMENTARY DATA

Supplementary data associated with this article can be found, in the online version, at http://dx.doi.org/10.1016/j.gca.2014.11.003.

REFERENCES

Affek H. and Eiler J. (2006) Abundance of mass 47 CO_2 in urban air, car exhaust, and human breath. *Geochim. Cosmochim. Acta* **70**, 1–12.

Azmy K., Lavoie D., Wang Z., Brand U., Al-Aasm I., Jackson S. and Girard I. (2013) Magnesium isotope and REE composition of Lower Ordovician carbonates from eastern Laurentia: Implications for the origin of dolomites and limestones. *Chem. Geol.* **356**, 64–75.

Banner J. L. (1995) Application of the trace element and isotope geochemistry of strontium to studies of carbonate diagenesis. *Sedimentology* **42**, 805–824.

Beinlich A., Mavromatis V., Austrheim H. and Oelkers E. H. (2014) Inter-mineral Mg isotope fractionation during hydrothermal ultramafic rock alteration – Implications for the global Mg-cycle. *Earth Planet. Sci. Lett.* **392**, 166–176.

Bjorlykke K. and Jahren J. (2012) Open or closed geochemical systems during diagenesis in sedimentary basins: Constraints on mass transfer during diagenesis and the prediction of porosity in sandstone and carbonate reservoirs. *Am. Assoc. Pet. Geol. Bull.* **96**, 2193–2214.

Bolou-Bi E. B., Vigier N., Brenot A. and Poszwa A. (2007) Compared magnesium isotope compositions of plants, rocks and waters. *Geochim. Cosmochim. Acta* **71**, 106.

Bolou-Bi E. B., Vigier N., Brenot A. and Poszwa A. (2009) Magnesium isotope compositions of natural reference materials. *Geostand. Geoanal. Res.* **33**, 95–109.

Bolou-Bi E. B., Poszwa A., Leyval C. and Vigier N. (2010) Experimental determination of magnesium isotope fractionation during higher plant growth. *Geochim. Cosmochim. Acta* **74**, 2523–2537.

Bontognali T. R. R., Vasconcelos C., Warthmann R. J., Bernasconi S. M., Dupraz C., Strohmenger C. J. and McKenzie J. A. (2010) Dolomite formation within microbial mats in the coastal sabkha of Abu Dhabi (United Arab Emirates). *Sedimentology* **57**, 824–844.

Bosellini A. (1998) *Geologie der Dolomiten*. Bozen, Arthesia, pp. 192.

Brenot A., Cloquet C., Vigier N., Carignan J. and France-Lanord C. (2008) Magnesium isotope systematics of the lithologically varied Moselle river basin, France. *Geochim. Cosmochim. Acta* **72**, 5070–5089.

Briere P. R. (2000) Playa, playa lake, sabkha: Proposed definitions for old terms. *J. Arid Environ.* **45**, 1–7.

Broecker W. S. and Peng T.-H. (1982) *Tracers in the Sea*. Lamont-Doherty Geological Observatory, Colombia University, Palisades, NY, 10964.

Budd D. A. (1997) Cenozoic dolomites of carbonate islands: Their attributes and origin. *Earth Sci. Rev.* **42**, 1–47.

Buhl D., Immenhauser A., Smeulders G., Kabiri L. and Richter D. K. (2007) Time series δ^{26}Mg analysis in speleothem calcite: Kinetic versus equilibrium fractionation, comparison with other proxies and implications for palaeoclimate research. *Chem. Geol.* **244**, 715–729.

Cander H. S., Kaufman J., Daniels L. D. and Meyers W. J. (1988) Regional dolomitization of shelf carbonates in the Burlington-Keokuk Formation (Mississippian), Illinois and Missouri: Constraints from cathodoluminescent zonal stratigraphy. In *Sedimentology and Geochemistry of Dolostones* (eds. V. Shukla and P. A. Baker). Society of Economic Paleontology and Mineralogy Special Publication, pp. 129–144.

Cerling E. T. and Quade J. (1993) Stable carbon and oxygen isotopes in soil carbonates. Climate change in continental isotopic records. *Geophys. Monogr.* **78**, 217–231.

Chafetz H. S. and Rush P. F. (1994) Diagenetically altered sabkha-type Pleistocene dolomite from the Arabian Gulf. *Sedimentology* **41**, 409–421.

Chakrabarti R. and Jacobsen S. B. (2010) The isotopic composition of magnesium in the inner Solar System. *Earth Planet. Sci. Lett.* **293**, 349–358.

Chang V. T.-C., Masishima A., Belshaw N. S. and ONions R. K. (2003) Purification of Mg from low Mg biogenic carbonates for isotope ratio determination using multi-collector ICP-MS. *J. Anal. At. Spectrom.* **18**, 296–301.

Chaudhuri S. and Clauer N. (1993) Strontium isotopic compositions and potassium and rubidium contents of formation waters in sedimentary basins: Clues to the origin of the solutes. *Geochim. Cosmochim. Acta* **57**, 429–437.

Czerniakowski L. A., Lohmann K. C. and Wilson J. L. (1984) Closed-system marine burial diagenesis; isotopic data from the Austin Chalk and its components. *Sedimentology* **31**, 863–877.

Davies G. R. and Smith L. B. (2006) Structurally controlled hydrothermal dolomite reservoir facies: An overview. *Am. Assoc. Pet. Geol.* **90**, 1641–1690.

De Deckker P. and Last W. M. (1988) Modern dolomite deposition in continental, saline lakes, western Victoria, Australia. *Geology* **16**, 29–32.

De Villiers S., Dickson J. A. D. and Ellam R. M. (2005) The composition of the continental river weathering flux deduced from seawater Mg isotopes. *Chem. Geol.* **216**, 133–142.

Dennis K. J. and Schrag D. P. (2010) Clumped isotope thermometry of carbonatites as an indicator of diagenetic alteration. *Geochim. Cosmochim. Acta* **74**, 4110–4122.

Dennis K. J., Affek H. P., Passey B. H., Schrag D. P. and Eiler J. M. (2011) Defining an absolute reference frame for 'clumped' isotope studies of CO_2. *Geochim. Cosmochim. Acta* **75**, 7117–7131.

Drummond J. M. (1964) An appraisal of fracture porosity. *Bull. Can. Pet. Geol.* **12**, 226–245.

Dupraz C., Reid R. P., Braissant O., Decho A. W., Norman R. S. and Visscher P. T. (2009) Processes of carbonate precipitation in modern microbial mats. *Earth Sci. Rev.* **96**, 141–162.

Eiler J. M. (2011) Paleoclimate reconstruction using carbonate clumped isotope thermometry. *Quatern. Sci. Rev.* **30**, 3575–3588.

Faure G. and Powell J. L. (1972) *Strontium Isotope Geology. Minerals, Rocks and Inorganic Materials*. Springer Verlag, Berlin, Heidelberg, New York, pp. 188.

Fantle M. S. and Higgins J. (2014) The effects of diagenesis and dolomitization on Ca and Mg isotopes in marine platform carbonates: Implications for the geochemical cycles of Ca and Mg. *Geochim. Cosmochim. Acta* **142**, 458–481.

Ferry J. M., Passey B. H., Vasconcelos C. and Eiler J. M. (2011) Formation of dolomite at 40–80 C in the Latemar carbonate

buildup, Dolomites, Italy, from clumped isotope thermometry. *Geology* **39**, 571–574.

Foster G. L., Pogge von Strandmann P. A. E. and Rae J. W. B. (2010) Boron and magnesium isotopic composition of seawater. *Geochem. Geophys. Geosyst.* **11**. http://dx.doi.org/10.1029/2010GC003201.

Frisia S. (1994) Mechanisms of complete dolomitization in a carbonate shelf: Comparison between the Norian Dolomia Principale (Italy) and the Holocene of Abu Dhabi Sabkha. In *Dolomites – A Volume in Honour of Dolomieu* (eds. B. Purser, M. Tucker and D. Zenger). Blackwell Scientific Publications, International Association of Sedimentologists, Special, Publication, pp. 55–89.

Füchtbauer H. and Goldschmidt H. (1965) Beziehungen zwischen Calcium-Gehalt und Bildungsbedingungen der Dolomite. *Geologische Rundschau* **55**, 29–40, Stuttgart.

Füchtbauer H. and Richter D. K. (1988) Karbonatgesteine. In *Sedimente und Sedimentgesteine* (ed. H. Füchtbauer). Stuttgart. pp. 233–434.

Galy A., Belshaw N. S., Halicz L. and O'Nions R. K. (2001) High-precision measurements of magnesium isotopes by multiple-collector inductively coupled plasma mass spectrometry. *Int. J. Mass Spectrom.* **208**, 89–98.

Galy A., Bar-Matthews M., Halicz L. and O'Nions R. K. (2002) Mg isotopic composition of carbonate: Insight from speleothem formation. *Earth Planet. Sci. Lett.* **201**, 105–115.

Galy A. Y. O., Janney P. E., Williams R. W., Cloquet C., Alard O., Halicz L., Wadwha M., Hutcheon I. D., Ramon E. and Carignan J. (2003) Magnesium isotopes heterogeneity of the isotopic standard SRM980 and new reference materials for magnesium-isotope-ratio measurements. *J. Anal. At. Spectrom.* **18**, 1352–1356.

Galy A., Carder E. and Elderfield H. (2006) Insights from magnesium isotopic compositions on the Oceanic Hydrothermal Circulation: Is seamount weathering the solution? In *American Geophysical Union*, Fall Meeting 2006, San Francisco, CA, USA.

Geske A., Zorlu J., Richter D. K., Buhl D., Niedermayr A. and Immenhauser A. (2012) Impact of diagenesis and low grade-metamorphosis on isotope (δ^{26}Mg, δ^{13}C, δ^{18}O and ^{87}Sr/^{86}Sr) and elemental (Ca, Mg, Mn, Fe and Sr) signatures of Triassic sabkha dolomites. *Chem. Geol.* **332–333**, 45–64.

Gillhaus A., Richter D., Götte T. and Neuser R. D. (2010) From tabular to rhombohedral dolomite crystals in Zechstein 2 dolostones from Schwarzfeld (SW Harz/Germany): A case study with combined CL and EBSD investigations. *Sed. Geol.* **228**, 284–291.

Gregg J. M. and Sibley D. F. (1984) Epigenetic dolomitization and the origin of xenotopic dolomite texture. *J. Sediment. Res.* **54**, 908–931.

Hardy R. and Tucker M. (1988) X-ray powder diffraction of sediments. In *Techniques in Sedimentology* (ed. M. E. Tucker). Blackwell Scientific Publications, Oxford, pp. 191–228.

Hiemstra E. J. and Goldstein R. H. (2004) The Indian Basin, New Mexico: A tectonically valved hydrothermal dolomite reservoir. In *American Association of Petroleum Geologists Annual Meeting*. AAPG Search and Discovery Article, Dallas, Texas.

Hiemstra E. J. and Goldstein R. H. (2014) Repeated injection of hydrothermal fluids into downdip carbonates: A diagenetic and stratigraphic mechanism for localization of reservoir porosity, Indian Basin field, New Mexico, USA. In *Fundamental Controls on Fluid Flow in Carbonates: Current Workflows to Emerging Technologies, Geol. Soc. London Special Publication*, vol. 406 (eds. S. Agar and S. Geiger). http://dx.doi.org/10.1144/SP406.1.

Higgins J. A. and Schrag D. P. (2010) Constraining magnesium cycling in marine sediments using magnesium isotopes. *Geochim. Cosmochim. Acta* **74**, 5039–5053.

Higgins J. A. and Schrag D. P. (2012) Records of Neogene seawater chemistry and diagenesis in deep-sea carbonate sediments and pore fluids. *Earth Planet. Sci. Lett.* **357–358**, 386–396.

Hill C. A. (1996) *Geology of the Delaware Basin: Guadalupe, Apache, and Glass Mountains*. Permian Basin Section, Society for Sedimentary Geology, New Mexico and West Texas, pp. 480.

Hippler D., Buhl D., Witbaard R., Richter D. K. and Immenhauser A. (2009) Towards a better understanding of magnesium-isotope ratios from marine skeletal carbonates. *Geochim. Cosmochim. Acta* **73**, 6134–6146.

Huang F., Glessner J., Ianno A., Lundstrom C. and Zhang Z. (2009) Magnesium isotopic composition of igneous rock standards measured by MC-ICP-MS. *Chem. Geol.* **268**, 15–23.

Huang K.-J., Teng F.-Z., Wei G.-J., Ma J.-L. and Bao Z.-Y. (2012) Adsorption- and desorption-controlled magnesium isotope fractionation druing extreme weathering of basalt in Hainan Island, China. *Earth Planet. Sci. Lett.* **359–360**, 73–83.

Huang K.-J., Teng F.-Z., Elsenouy A., Li W.-L. and Bao Z.-Y. (2013) Magnesium isotopic variations in loess: Origins and implications. *Earth Planet. Sci. Lett.* **374**, 60–70.

Humphrey J. D. and Quinn T. M. (1989) Coastal marine altered dolomite, forward modeling, and massive dolomitization of platform-margin carbonates. *J. Sediment. Res.* **59**, 438–454.

Huntington K. W., Eiler J. M., Affek H. P., Guo W., Bonifacie M., Yeung L. Y., Thiagarajan N., Passey B., Tripati A., Daeron M. and Came R. (2009) Methods and limitations of "clumped" CO_2 isotope (Δ_{47}) analysis by gassource isotope ratio mass spectrometry. *J. Mass Spectrom.* **44**, 1318–1329.

Huntington K. W., Budd D. A., Wernicke B. P. and Eiler J. M. (2011) Use of clumped-isotope thermometry to constrain the crystallization temperature of diagenetic calcite. *J. Sediment. Res.* **81**, 656–669.

Immenhauser A., Buhl D., Richter D., Niedermayr A., Riechelmann D., Dietzel M. and Schulte U. (2010) Magnesium-isotope fractionation during low-Mg calcite precipitation in a limestone cave – Field study and experiments. *Geochim. Cosmochim. Acta* **74**, 4346–4364.

Irwin H., Curtis C. and Coleman M. (1977) Isotopic evidence for source of diagenetic carbonates formed during burial of organic-rich sediments. *Nature* **269**, 209–213.

Jacobson A. D., Zhang Z., Lundstrom C. and Huang F. (2010) Behavior of Mg isotopes during dedolomitization in the Madison Aquifer, South Dakota. *Earth Planet. Sci. Lett.* **297**, 446–452.

Jaffrés J. B. D., Shields G. A. and Wallmann K. (2007) The oxygen isotope evolution of seawater: A critical review of a long-standing controversy and an improved geological water cycle model for the past 3.4 billion years. *Earth Sci. Rev.* **83**, 83–122.

Jones G. D. and Xiao Y. (2005) Dolomitization, anhydrite cementation, and porosity evolution in a reflux system: Insights from reactive transport models. *Am. Assoc. Pet. Geol. Bull.* **89**, 577–601.

Kasemann S. A., Pogge von Strandmann P. A. E., Prave A. R., Fallick A. E., Elliott T. and Hoffmann K.-H. (2014) Continental weathering following a Cryogenian glaciation: Evidence from calcium and magnesium isotopes. *Earth Planet. Sci. Lett.* **396**, 66–77.

Kesler S. E., Martini A. M., Appold M. S., Walter L. M., Huston T. J. and Furman F. C. (1996) Na–Cl–Br systematics of fluid inclusions from Mississippi Valley-type deposits, Appalachian

Basin: Constraints on solute origin and migration paths. *Geochim. Cosmochim. Acta* **60**, 225–233.

Kisakurek B., Niedermayr A., Moeller M. N., Taubner I., Eisenhauer A., Dietzel M., Buhl D., Fietzke J. and Erez J. (2009) Magnesium isotope fractionation of inorganic and biogenic calcite. *Geochim. Cosmochim. Acta* **73**, A663.

Koch R. and Schorr M. (1986) Diagenesis of Upper Jurassic sponge-algal reefs in SW Germany. In *Reef Diagenesis* (eds. H. Schroeder and B. H. Purser). Springer, Berlin Heidelberg, p. 468.

Land L. S. (1980) The isotopic and trace element geochemistry of dolomite: The state of the art. In *Concepts and Models of Dolomitization* (eds. D. H. Zenger, J. B. Dunham and R. L. Ethington). SEPM Society for Sedimentary Research Special, Publication, pp. 87–110.

Last W. M. (1990) Lacustrine dolomite—an overview of modern, Holocene, and Pleistocene occurrences. *Earth Sci. Rev.* **27**, 221–263.

Last F. M., Last W. M. and Halden N. M. (2010) Carbonate microbialites and hardgrounds from Manito Lake, an alkaline, hypersaline lake in the northern Great Plains of Canada. *Sed. Geol.* **225**, 34–49.

Last F. M., Last W. M. and Halden N. M. (2012) Modern and late Holocene dolomite formation: Manito Lake, Saskatchewan, Canada. *Sed. Geol.* **281**, 222–237.

Lavoie D., Jackson S. and Girard I. (2014) Magnesium isotopes in high-temperature saddle dolomite cements in the lower Paleozoic of Canada. *Sed. Geol.* **305**, 58–68.

Lohmann K. C. (1978) Closed system diagenesis of high magnesium calcite and aragonite cement. *Geol. Soc. Am. Abst. Programs* **10**, 446.

Liu S.-A., Teng F.-Z., He Y., Ke S. and Li S. (2010) Investigation of magnesium isotope fractionation during granite differentiation: Implication for Mg isotopic composition of the continental crust. *Earth Planet. Sci. Lett.* **297**, 646–654.

Li W.-Y., Chakraborty S., Beard B. I., Romanek C. S. and Johnson V. M. (2012a) Magnesium isotope fractionation during precipitation of inorganic calcite under laboratory conditions. *Earth Planet. Sci. Lett.* **333–334**, 304–316.

Li W.-Y., Chakraborty S., Beard B. L., Romanek C. S. and Johnson C. M. (2012b) Temperature-dependent Mg isotope fractionation during precipitation of inorganic calcite under laboratory conditions. *Earth Planet. Sci. Lett.* **333–334**, 304–316.

Li Z., Goldstein R. H. and Franseen E. K. (2013) Ascending freshwater-mesohaline mixing: A new scenario for dolomitization. *J. Sediment. Res.* **83**, 277–283.

Li W., Beard B. L., Li C. and Johnson C. M. (2014a) Magnesium isotope fractionation between brucite (Mg(OH)2) and Mg aqueous species: Implication for silicate weathering and biogeochemical processes. *Earth Planet. Sci. Lett.* **394**, 82–93.

Li W.-Y., Teng F.-Z., Wing B. A. and Xiao Y. (2014b) Limited magnesium isotope fractionation during metamorphic dehydration in metapelites from the Onawa contact aureole, Maine. *Geochem. Geophys. Geosyst.*. http://dx.doi.org/10.1002/20GC004992.

Ling M.-X., Sedaghatpour F., Teng F.-Z., Hays P. D., Strauss J. and Sun W. (2011) Homogeneous magnesium isotopic composition of seawater: An excellent geostandard for Mg isotope analysis. *Rapid Commun. Mass Spectrom.* **25**, 2828–2836.

Lokier S. and Steuber T. (2009) Large-scale intertidal polygonal features of the Abu Dhabi coastline. *Sedimentology* **56**, 609–621.

Lokier S., Knaf A. and Kimiagar S. (2013) A quantitative analysis of recent arid coastal sedimentary facies from the Arabian Gulf Coastline of Abu Dhabi, United Arab Emirates. *Marine Geol.* **346**, 141–152.

Lowenstam H. and Epstein S. (1957) On the origin of sedimentary aragonite needles of Great Bahama Bank. *J. Geol.* **65**, 364–375.

Lumsden D. N. (1979) Discrepancy between thin section and X-ray estimates of dolomite in limestone. *J. Sediment. Petrol.* **49**, 429–436.

M'Rabet A. (1981) Differentiation of environments of environments of dolomite formation, Lower Cretaceous of Central Tunisia. *Sedimentology* **28**, 331–352.

Machel H. G. (1987) Saddle dolomite as a by-product of chemical compaction and thermochemical sulfate reduction. *Geology* **15**, 936–940.

Machel H. G. (2004) Concepts and models of dolomitization: A critical reappraisal. In *The Geometry and Petrogenesis of Dolomite Hydrocarbon Reservoirs* (eds. C. J. R. Braithwaite, G. Rizzi and G. Darke). Geological Society, Special Publication, London, pp. 7–63.

Machel H. G. (2013) Secondary anhydrites in deeply buried Devonian carbonates of the Alberta Basin, Canada. *Carbonates Evaporites* **28**, 267–280.

Machel H. G. and Anderson J. H. (1989) Pervasive subsurface dolomitization of the Nisku formation in Central Alberta. *J. Sediment. Petrol.* **59**, 891–911.

Machel H. G. and Lonnee J. (2002) Hydrothermal dolomite – A product of poor definition and imagination. *Sed. Geol.* **152**, 163–171.

Machel H. G., Krouse H. R. and Sassen R. (1995) Products and distinguishing criteria of bacterial and thermochemical sulfate reduction. *Appl. Geochem.* **10**, 373–389.

Malone M. J., Baker P. A. and Burns S. J. (1996) Hydrothermal dolomitization and recrystallization of dolomite breccias from the Miocene Monterey Formation, Tepusquet Area, California. *J. Sediment. Res.* **66**, 976–990.

Mattes B. W. and Mountjoy E. W. (1980) Burial dolomitization of the Upper Devonian Miette Buildup, Jasper National Park, Alberta. In *Concepts and Models of Dolomitization* (eds. D. H. Zenger, J. B. Dunham and R. L. Ethington). Society of Economic Paleontology and, Mineralogy, pp. 259–297.

Matthews A. and Katz A. (1977) Oxygen isotope fractionation during the dolomitization of calcium carbonate. *Geochim. Cosmochim. Acta* **41**, 1431–1438.

Mavromatis V., Pearce R. C., Shirokova L. S., Bundeleva I. A., Pokrovsky O. S., Benezeth P. and Oelkers E. H. (2012) Magnesium isotope fractionation during hydrous magnesium carbonate precipitation with and without cyanobacteria. *Geochim. Cosmochim. Acta* **76**, 161–174.

Mavromatis V., Gautier Q., Bosc O. and Schott J. (2013) Kinetics of Mg partition and Mg stable isotope fractionation during its incorporation in calcite. *Geochim. Cosmochim. Acta* **114**, 188–203.

Mavromatis V., Meister P. and Oelkers E. H. (2014) Using stable Mg isotopes to distinguish dolomite formation mechanisms: A case study from the Peru Margin. *Chem. Geol.* **385**, 84–91.

Mazzullo S. J. (2000) Organogenic dolomitization in peritidal to deep-sea sediments. *J. Sediment. Res.* **70**, 10–23.

Melim L. A., Westphal H., Swart P. K., Eberli G. P. and Munnecke A. (2002) Questioning carbonate diagenetic paradigms: Evidence from the Neogene of the Bahamas. *Mar. Geol.* **185**, 27–53.

Meyer R. K. F. and Schmidt-Kaler H. (1990) Paläogeographie und Schwammriff-Entwicklung des süddeutschen Oberjura (Malm) – Ein Überblick. *Facies* **23**, 175–184.

McArthur J. M., Howarth R. J. and Bailey T. R. (2001) Strontium isotope stratigraphy: LOWESS Version 3; best fit to the marine

Sr-isotope curve for 0–509Ma and accompanying look-up tabe for deriving numerical age. *J. Geol.* **109**, 155–170.
McKenzie J. A. (1981) Holocene dolomitization of calcium carbonate sediments from the coastal sabkhas of Abu Dhabi, U.A.E.: A stable isotope study. *J. Geol.* **89**, 185–198.
Milliman J. D. (1974) *Marine Carbonates*. Springer, Berlin, pp. 375.
Morrow D. W. (1982) Diagenesis 2. Dolomite – Part 2 Dolomitization models and ancient dolostones. *Geosci. Can.* **9**, 95–107.
Morse J. W. and Arvidson R. S. (2002) The dissolution kinetics of major sedimentary carbonate minerals. *Earth Sci. Rev.* **58**, 51–84.
Murray R. C. (1960) Origin of porosity in carbonate rocks. *J. Sediment. Petrol.* **30**, 59–84.
Müller D. W., McKenzie J. A. and Mueller P. A. (1990) Abu Dhabi sabkha, Persian Gulf, revisited: Application of strontium isotopes to test an early dolomitization model. *Geology* **18**, 618–621.
Neuser R. D., Bruhn F., Götze J., Habermann D. and Richter D. K. (1996) Kathodolumineszenz: Methodik und Anwendung. *Zbl. Geol. Paläontol.* **1**, 287–306.
Opfergelt S., Georg R. B., Delvaux B., Cabidoche Y.-M. and Halliday A. N. (2012) Mechanism of magnesium isotope fractionation in volcanic soil weathering sequences, Guadeloupe. *Earth Planet. Sci. Lett.* **341–344**, 176–185.
Passey B. H. and Henkes G. A. (2012) Carbonate clumped isotope bond reordering and geospeedometry. *Earth Planet. Sci. Lett.* **351–352**, 223–236.
Paulo C. and Dittrich M. (2013) 2D Raman spectroscopy study of dolomite and cyanobacterial extracellular polymeric substances from Khor Al-Adaid sabkha (Qatar). *J. Raman Spectrosc.* **44**, 1563–1569.
Pearce C. R., Saldi G. D., Schott J. and Oelkers E. H. (2012) Isotopic fractionation during congruent dissolution, precipitation and at equilibrium: Evidence from Mg isotopes. *Geochim. Cosmochim. Acta* **92**, 170–183.
Pogge von Strandmann P. A. E., James R. H., van Calsteren P., Gislason S. R. and Burton K. W. (2008a) Lithium, magnesium and uranium isotope behaviour in the estuarine environment of basaltic islands. *Earth Planet. Sci. Lett.* **274**, 462–471.
Pogge von Strandmann P. A. E., Burton K. W., James R. H., Van Calsteren P., Gislason S. R. and Sigfusson B. (2008b) The influence of weathering processes on riverine magnesium isotopes in a basaltic terrain. *Earth Planet. Sci. Lett.* **276**, 187–197.
Pogge von Strandmann P. A. E., Forshaw J. and Schmidt D. N. (2014) Modern and Cenozoic records of seawater magnesium from foraminiferal Mg isotopes. *Biogeosciences* **11**, 5155–5168.
Pokrovsky B. G., Mavromatis V. and Pokrovsky O. S. (2011) Co-variation of Mg and C isotopes in late Precambrian carbonates of the Siberian Platform: A new tool for tracing the change in weathering regime? *Chem. Geol.* **290**, 67–74.
Purser B. H. and Sibold E. (1973) The principal environmental factors influencing Holocene sedimentation and diagenesis in the Persian Gulf. In *The Persian Gulf* (ed. B. H. Purser). Springer, New York, pp. 1–9.
Radke B. M. and Mathis R. L. (1980) On the formation and occurrence of saddle dolomite. *J. Sediment. Petrol.* **50**, 1149–1168.
Reinhold C. (1998) Multiple episodes of dolomitization and dolomite recrystallization during shallow burial in Upper Jurassic shelf carbonates: Eastern Swabian Alb, southern Germany. *Sed. Geol.* **121**, 71–95.
Richter D. K. (1974) Entstehung und Diagenese der devonischen und permotriassischen Dolomite der Eifel. *Contrib. Sedimentol.* **2**, 1–101.
Richter D. K., Götte T., Götze J. and Neuser R. D. (2003a) Progress in application of cathodoluminescence (CL) in sedimentary petrology. *Mineral. Petrol.* **79**, 127–166.
Richter D. K., Gillhaus A. and Götte T. (2003b) Kathodolumineszenzuntersuchungen zur polyphasen Entwicklung des Frankendolomits (Malm, E-Bayern). *Terra Nostra* **3**, 133–134.
Richter D. K., Heinrich F., Geske A., Neuser R. D., Gies H. and Immenhauser A. (2014) First description of Phanerozoic radiaxial fibrous calcites. *Sed. Geol.* **304**, 1–10.
Riechelmann D. F. C., Niggemann S., Richter D. K. and Spötl C. (2009) Mehrjähriges Monitoring in der Bunkerhöhle (Sauerland, NRW): Methodik und erste Ergebnisse. *Mitteilungen der Verbindung deutscher Höhlen und Karstforschung* **2**, 44–52.
Riechelmann S., Buhl D., Schröder-Ritzrau A., Riechelmann D. F. C., Richter D. K., Vonhof H. B., Wassenburg J. A., Geske A., Spötl C. and Immenhauser A. (2012a) The magnesium isotope record of cave carbonate archives. *Clim. Past* **8**, 1849–1867.
Riechelmann S., Buhl D., Schröder-Ritzrau A., Spötl C., Riechelmann D. F. C., Richter D. K., Kluge T., Marx T. and Immenhauser A. (2012b) Hydrogeochemistry and fractionation pathways of Mg isotopes in a continental weathering system: Lessons from field experiments. *Chem. Geol.* **300–301**, 109–122.
Roberts J., Kenward P. A., Fowle D. A., Goldstein R. H., González L. A. and Moore D. S. (2013) Surface chemistry allows for abiotic precipitation of dolomite at low temperature. *Proc. Natl. Acad. Sci.* **110**, 14540–14545.
Schauble E. A. (2004) Applying stable isotope fractionation theory to new systems, Geochemistry of non-traditional stable isotopes. In *Geochemistry of Non-traditional Stable Isotopes* (eds. C.M. Johnson, B.L. Beard, F. Albaréde). *Reviews in Mineralogy and Geochemistry,* vol. 56. Mineralogical Society of America, Washington. pp. 65–111.
Schauble E. A. (2011) First-principles estimates of equilibrium magnesium isotope fractiontation in silicate, oxide, carbonate and hexaaquamagnesium (2+) crystals. *Geochim. Cosmochim. Acta* **75**, 844–869.
Sibley D. F. and Gregg J. M. (1987) Classification of dolomite rock textures. *J. Sediment. Res.* **57**, 967–975.
Sibley D. F., Nordeng S. H. and Borkowski M. L. (1994) Dolomitization kinetics in hydrothermal bombs and natural settings. *J. Sediment. Res.* **64**, 630–637.
Shirokova L. S., Mavromatis V., Bundeleva I. A., Pokrovsky O. S., Benezeth P., Gerard E., Pearce C. R. and Oelkers E. H. (2013) Using Mg isotopes to trace cyanobacterially mediated magnesium carbonate precipitation in alkaline lakes. *Aquat. Geochem.* **19**, 1–24.
Spötl C. and Pitman J. K. (1998) Saddle (baroque) dolomite in carbonates and sandstones: A reappraisal of a burial-diagenetic concept. In *Carbonate Cementation in Sandstones: Distribution Patterns and Geochemical Evolution* (ed. M. Sadoon). Blackwell Science, International Association of Sedimentologists, Special Publication. pp. 437–460.
Stanley S. M. (2006) Influence of seawater chemistry on biomineralization throughout phanerozoic time: Paleontological and experimental evidence. *Palaeogeogr. Palaeoclimatol. Palaeoecol.* **232**, 214–236.
Suzuki Y., Iryu Y., Inagaki S., Yamada T., Aizawa S. and Budd D. A. (2006) Origin of atoll dolomites distinguished by geochemistry and crystal chemistry: Kita-daito-jima, northern Philippine Sea. *Sed. Geol.* **183**, 181–202.
Swart P. K., Cantrell D. L., Westphal H., Handford R. and Kendall C. G. (2005) Origin of dolomite in the Arab-D reservoir from the Ghawar field, Saudi Arabia: Evidence from petrographic and geochemical constraints. *J. Sediment. Res.* **75**, 476–491.

Teng F.-Z., Li W.-Y., Ke S., Marty B., Dauphas N., Huang S., Wu F.-Y. and Pourmand A. (2010) Magnesium isotopic composition of the Earth and chondrites. *Geochim. Cosmochim. Acta* **74**, 4150–4166.

Tipper E. T., Bickle M. J., Galy A., West J., Pomiés C. and Chapman H. J. (2006a) The short term sensitivity of carbonates and silicate weathering fluxes: Insight from seasonal variations in river chemistry. *Geochim. Cosmochim. Acta* **70**, 2737–2754.

Tipper E. T., Galy A. and Bickle M. J. (2006b) Riverine evidence for a fractionated reservoir of Ca and Mg on the continents: Implications for the oceanic Ca cycle. *Earth Planet. Sci. Lett.* **247**, 267–279.

Tipper E. T., Galy A., Gaillardet J., Bickle M. J., Elderfield H. and Carder E. A. (2006c) The magnesium isotope budget of the modern ocean: Constraints from riverine magnesium isotope ratios. *Earth Planet. Sci. Lett.* **250**, 241–253.

Tipper E. T., Galy A. and Bickle M. J. (2008a) Calcium and magnesium isotope systematics in rivers draining the Himalaya-Tibetan-Plateau region: Lithological or fractionation control? *Geochim. Cosmochim. Acta* **72**, 1057–1075.

Tipper E. T., Louvat P., Capmas F., Galy A. and Gaillardet J. (2008b) Accuracy of stable Mg and Ca isotope data obtained by MC-ICP-MS using the standard addition method. *Chem. Geol.* **257**, 65–75.

Tipper E. T., Lemarchand E., Hindshaw R. S., Reynolds B. C. and Bourdon B. (2012) Seasonal sensitivity of weathering processes: Hints from magnesium isotopes in a glacial stream. *Chem. Geol.* **312–313**, 80–92.

Tucker M. E. and Wright V. P. (1990) *Carbonate Sedimentology*. Blackwell Science, Oxford, pp. 482.

Vahrenkamp V. C. and Swart P. K. (1990) New distribution coefficient for the incorporation of strontium into dolomite and its implications for the formation of ancient dolomites. *Geology* **18**, 387–391.

Van Lith Y., Warthmann R., Vasconcelos C. and McKenzie J. A. (2003b) Sulphate-reducing bacteria induce low-temperature Ca-dolomite and high Mg-calcite formation. *Geobiology* **1**, 71–79.

Vasconcelos C., McKenzie J. A., Bernasconi S., Grujic D. and Tien A. J. (1995) Microbial mediation as a possible mechanism for natural dolomite formation at low temperatures. *Nature* **377**, 220–222.

Vasconcelos C., McKenzie J. A., Warthmann R. and Bernasconi S. M. (2005) Calibration of the $\delta^{18}O$ paleothermometer for dolomite precipitated in microbial cultures and natural environments. *Geology* **33**, 317–320.

Watson E. B. and Baxter E. F. (2007) Diffusion in solid-Earth systems. *Earth Planet. Sci. Lett.* **253**, 307–327.

Wallace M. W. (1990) Origin of dolomitization on the Barbwire Terrace, Canning Basin, Western Australia. *Sedimentology* **37**, 105–123.

Wang Z., Hu P., Gaetani G., Liu C., Saenger C., Cohen A. and Hart S. (2013) Experimental calibration of Mg isotope fractionation between aragonite and seawater. *Geochim. Cosmochim. Acta* **102**, 113–123.

Warren J. (2000) Dolomite: Occurrence, evolution and economically important associations. *Earth Sci. Rev.* **52**, 1–81.

Wassenburg J. A., Immenhauser A., Richter D. K., Niedermayr A., Riechelmann S., Fietzke J., Scholz D., Jochum K. P., Fohlmeister J., Schröder-Ritzrau A., Sabaoui A., Riechelmann D. F. C., Schneider L. and Esper J. (2013) Moroccan speleothem and tree ring records suggest a variable positive state of the North Atlantik Oscillation during the Medieval Warm Period. *Earth Planet. Sci. Lett.* **375**, 291–302.

Wimpenny J., Burton K. W., James R. H., Gannoun A., Mokadem F. and Gislason S. R. (2011) The behaviour of magnesium and its isotopes during glacial weathering in an ancient shield terrain in West Greenland. *Earth Planet. Sci. Lett.* **304**, 260–269.

Wimpenny J., Colla C. A., Yin Q.-Z., Rustad J. R. and Casey W. H. (2014a) Investigation the behaviour of Mg isotopes during the formation of clay minerals. *Geochem. Cosmochim. Acta* **182**, 178–194.

Wimpenny J., Yin Q.-Z. and Tollstrup D. (2014b) Using Mg isotope ratios to trace Cenozoic weathering changes: A case study from the Chinese loess plateau. *Chem. Geol.*, 31–43.

Wombacher F., Eisenhauer A., Heuser A. and Weyer S. (2009) Separation of Mg, Ca and Fe from geological reference materials for stable isotope ratio analyses by MC-ICP-MS and double-spike TIMS. *J. Anal. At. Spectrom.* **24**, 627–636.

Wombacher F., Eisenhauer A., Böhm F., Gussone N., Regenberg M., Dullo W.-Chr. and Rüggeberg A. (2011) Magnesium stable isotope fractionation in marine biogenic calcite and aragonite. *Geochim. Cosmochim. Acta* **75**, 5797–5818.

Yoshimura T., Tanimizu M., Inoue M., Suzuki A., Iwasaki N. and Kawahata H. (2011) Mg isotope fractionation in biogenic carbonates of deep-sea coral, benthic foraminifera, and hermatypic coral. *Anal. Bioanal. Chem.* **401**, 2755–2769.

Young E. D. and Galy A. (2004) The isotope geochemistry and cosmochemistry of Magnesium. *Rev. Mineral. Geochem.* **55**, 197–230.

Zhang F., Xu H., Konishi H., Shelobolina E. S. and Roden E. E. (2012) Polysaccharide-catalyzed nucleation and growth of disordered dolomite: A potential precursor of sedimentary dolomite. *Am. Mineral.* **97**, 556–567.

Associate editor: Andrew D. Jacobson